WL-TDR-64-15

RE-ENTRY BURN-UP MODEL FOR A
HYDRIDED ZIRCONIUM-URANIUM FUEL ELEMENT

TECHNICAL DOCUMENTARY REPORT NO. WL-TDR-64-15

Final Report

June 1964

Research and Technology Division
AIR FORCE WEAPONS LABORATORY
Air Force Systems Command
Kirtland Air Force Base
New Mexico

Project No. 1831, Task No. 183101

(Prepared under Contract AF 29(601)-5907
by H. M. Childers, L. C. McCandless,
and H. S. Jacobs, General Technologies
Corporation, 708 North West Street,
Alexandria, Virginia)

NO OTS

Research and Technology Division
Air Force Systems Command
AIR FORCE WEAPONS LABORATORY
Kirtland Air Force Base
New Mexico

FOREWORD

ABSTRACT

The problem of describing the re-entry behavior of a hydrided zirconium-uranium fuel element of the SNAP 2 and 10A variety in an analytical form suitable for computer application is studied with special emphasis placed on the chemical interactions of the fuel with the re-entry environment. General re-entry equations are presented. The trajectory and angular-motion equations are written in a form that includes effects from transpiration cooling, heats of fusion, evaporation, dissociation, recombination, chemical reactions, and mass accretion (or loss). All pertinent parameters are evaluated insofar as available data will permit. The rate of hydrogen transpiration, the heat energy added to the fuel element due to recombination of the transpired hydrogen, and the vapor pressure of molten fuel material could not be determined with reasonable accuracy from the available data. It is recommended that these three parameters be determined through laboratory experiments and used in the model described to determine whether or not the fuel elements will burn up during re-entry.

PUBLICATION REVIEW

This report has been reviewed and is approved.

RICHARD A. POURCIAU
Lieutenant   USAF
Project Officer

JOHN W. TALLEY
Lt Colonel   USAF
Chief, Nuclear Power Branch

RICHARD A. HOUSE
Colonel   USAF
Chief, Development Division

CONTENTS

LIST OF FIGURES

LIST OF TABLES

LIST OF SYMBOLS

a = hydrogen diffusion coefficient in ZrO_2 (grams/cm^2-min, see eq. 84)

A = cross sectional area of vehicle = ℓd (ft^2)

A_d = area of end of cylindrical rod = $\pi d^2/4$ (ft^2)

a_e = local velocity of sound = $\sqrt{\gamma R_g T_e}$ (ft/sec)

A_s = pre-factor in the Arrhenius equation (grams^2/cm^4-min)

b = arguments for the Bessel function

b_n = positive roots of the first order Bessel function $J_1(b) = 0$

B_1, B_2 = constants defined by eq. (23)

C = 2.27×10^{-8}

C^* = $\mu^* T^*/\mu_\infty T_\infty$ (see eq. 31)

$C^*(\phi)$ = $\mu^*(\phi)T_\infty/\mu_\infty T^*(\phi)$ (see eq. 39)

C_D = drag coefficient

C_{Dd} = drag coefficient for end face of rod

C_f = local skin friction coefficient

$\bar{C}_f$ = mean value of skin friction coefficient

C_H = heat transfer coefficient

C_{Hab} = heat transfer coefficient for afterbody

C_{Hs} = heat transfer coefficient at stagnation point

C_L = lift coefficient

C_p = specific heat capacity of constant pressure (Btu/slug-°R)

C_{pa} = specific heat capacity of air = 7.73 Btu/slug-°R

$\bar{C}_p$ = average specific heat capacity of rod material (Btu/slug-°R)

C_v = specific heat capacity at constant volume (Btu/slug-°R)

D = drag force = $\frac{1}{2} \rho_\infty V_\infty^2 C_D A$ (slug-ft/sec^2)

d = diameter of vehicle (ft)

ds = elementary segment of arc $(ds^2 = dx^2 + dy^2)$

$d\gamma$ = elementary angle subtended at the center of curvature of the trajectory by the elementary arc length of trajectory ds

$d\sigma$ = elementary angle subtended by ds as viewed from the center of the earth

F = function defined by eqs. (6a) and (7)

F_c = fraction of heat energy released by combustion or recombination of transpiring gas that is transferred to the fuel rod

F_v = fraction of fused material that is vaporized

g = acceleration of gravity = 32.2 ft/sec^2

$G(T_w)$ = functional relationship between T_w and dehydriding rate of fuel element

$H_{c,deG}$ = heat energy released in the combustion or recombination of the transpired gas (Btu/slug)

H_{ch} = heat of chemical reaction, e.g. H_{ZrO_2}, H_{ZrN} (Btu/gram-mole)

$\dot{H}_{ch}$ = rate of chemical heat energy release (Btu/ft^2-sec)

H_{deG} = heat energy required to release one slug of gas (Btu/slug)

h_e = enthalpy content of the gas at the outer edge of the boundary layer (Btu/slug)

H_f = heat of fusion (Btu/slug)

h_r = recovery enthalpy (see eq. 49) (Btu/slug)

h_{rod} = total enthalpy of rod (Btu)

h_s = stagnation enthalpy (Btu/slug)

H_v = heat of vaporization (Btu/slug)

h_w = enthalpy of gas at wall temperature (Btu/slug)

h_{wf} = enthalpy of gas at temperature T_{wf} (Btu/slug)

h_{wg} = enthalpy of gas at wall temperature T_{wg} (Btu/slug)

$h_{w_{300}}$ = enthalpy of gas at wall temperature 300°R

ix

h^* = reference enthalpy (see eq. 40)

h' = 272,234 Btu/slug (=8465 Btu/lb)

i = dummy index number

ı = moment of inertia (slug-ft^2)

J = mechanical equivalent of heat = 778 ft-lbs/Btu

K^2 = correlation parameter = $Re_\infty/Y_\infty M^2_\infty C^*$ (see eq. 30)

$K^2(\phi)$ = $Re_\infty/Y_\infty M^2_\infty C^*(\phi)\left|\sin\phi\right|$ (see eq. 38)

K = upper boundary condition on $K^2(\phi)$

$K'(Y)$ = constant (see eq. 52)

k_m = thermal conductivity of rod material (Btu/sec-ft-°R)

k_s = rate constant for parabolic oxidation law (grams^2/cm^4-min or lbs^2/ft^4-sec as appropriate)

ℓ = length of vehicle (ft)

L_1 = lift force = $\frac{1}{2}\rho_\infty V^2_\infty C_L A$ (slugs-ft/sec^2)

M = molecular weight of gas (grams/mole)

M_{ch} = molecular mass of chemical reactant or produce, e.g. M_{ZrO_2} (slugs/mole)

M_{deG} = gram molecular weight of transpiring gas (grams/mole)

M_{Ho} = hydrogen mass per unit surface area (grams/cm^2)

M_{Hr} = mass of hydrogen released per unit area in a time ı (grams/cm^2)

M_e = local Mach number at edge of boundary layer

M_r = molecular mass of rod material (slugs/mole)

M_∞ = free stream Mach number

Δm_s = change in mass (grams/cm^2 or lbs/ft^2 as appropriate)

Δm = mass of hydrogen in rod per unit area (grams/cm^2)

n = dummy index number and order of Jacobian

P_e = local Pitot pressure at outer edge of boundary layer (lbs/ft^2)

P_v = vapor pressure (mm Hg)

P_o' = normal shock recovery pressure (lbs/ft^2)

Pr = Prandtl number = $4\gamma/(9\gamma - 5)$

P_s = stagnation pressure (lbs/ft^2)

P_∞ = free stream pressure (lbs/ft^3)

$\dot{q}$ = heat flux (Btu/ft^2-sec)

$\dot{q}_a$ = average value of radial heat flux to cylinder = $0.31 \dot{q}_s$ (Btu/ft^2-sec)

$\dot{q}_{ab}$ = heat flux to afterbody of cylinder (Btu/ft^2-sec)

$\dot{q}_o$ = radial heat flux without transpiration cooling (Btu/ft^2-sec)

$\dot{q}_s$ = radial heat flux at stagnation point (Btu/ft^2-sec)

$\dot{q}_{tr}$ = radial heat flux with transpiration cooling (Btu/ft^2-sec)

$\dot{q}_1$ = radial heat flux into rod (Btu/ft^2-sec)

$\dot{q}_{1i}$ = normal heat flux through surface of fuel rod during i_th_ time interval (Btu/ft^2-sec)

r = distance between centers of gravity of earth and vehicle (ft)

r_c = radius of curvature of vehicle trajectory (ft)

Re = Reynolds number

$(R_e)_\ell$ = local value of Reynolds number = $\rho_e V_e \ell/\mu_e$

Re_∞ = $\rho_\infty V_\infty d/2\mu_\infty$ (applicable to end of cylinder)

R_g = universal gas constant = 1715 ft-lbs/slug$^\circ$R

r_g = radius of gyration (ft)

r_o = radius of earth (or reference sphere whose radius is the average value of the earth's radius) (ft)

$\vec{r_o}$ = vector from center of gravity of earth to center of gravity of vehicle

s = arc length, dummy index or refers to stagnation value as appropriate

Q_s = reaction energy divided by R_g ($^{\circ}R$)

S = area of vehicle, and initially $S = \pi d^2/2 + \pi d \ell$ (ft^2)

S^* = constant = 198.6

St = $\overline{C}_f \, Pr^{-2/3}/2$

T = absolute temperature ($^{\circ}R$)

t = time (seconds or minutes, as required)

T_e = local temperature at outer edge of boundary layer ($^{\circ}R$)

T_o = initial temperature of rod ($^{\circ}R$)

T_s = stagnation temperature $= V_{\infty}^2/2 \, J C_{pa}$ ($^{\circ}R$)

$\overline{T}$ = average temperature of the rod, e.g. $h_{rod} = \overline{C}_p \overline{T}$ ($^{\circ}R$)

$\overline{T}_{s-1}$ = average temperature of the rod during the time interval Δt_s ($^{\circ}R$)

T_w = wall temperature ($^{\circ}R$)

T_{wf} = wall temperature at time of fusion ($^{\circ}R$)

T_{wg} = wall temperature at time of gas transpiration ($^{\circ}R$)

T^* = reference temperature (see eqs. 32, 40)

Δt_s = short time interval, $s = 0, 1, 2 \ldots$

T_{∞} = free stream temperature ($^{\circ}R$)

V = velocity (ft/sec)

V_e = local stream velocity at outer edge of boundary layer $= a_e M_e$ (ft/sec)

V_{∞} = free stream velocity, hence vehicle velocity relative to stationary atmosphere (ft/sec)

W = local time weight of vehicle (lbs)

W_1 = weight gained or lost per unit area (lbs/ft^2 or grams/cm^2 as appropriate)

x = position coordinate of vehicle along surface of sphere whose radius is $y_E + r_o$ (ft)

x_e = position coordinate along surface of rod (distance reckoned from stagnation point in end-on flow condition) (ft)

$\bar{x}$ = radial distance from cylindrical axis of rod (ft)

y = altitude of vehicle (or distance above reference sphere) (ft)

y_E = altitude of vehicle (fuel element) at beginning of re-entry trajectory (ft)

Greek Symbols

α = 0.715

β = 1/(24,800 ft)

γ = specific heat capacity ratio = C_p/C_v

γ_∞ = free stream specific heat capacity ratio

Δt_i = short time interval $\sim$ 1 to 3 seconds, i = 0, 1, 2, 3... (sec)

ε = optical emittance of vehicle surface

ε^* = density ratio across normal shock

ζ = $(du/dx)_s$ = stagnation point velocity gradient (see eq. 63)

ζ_n = Newtonian value of ζ (see eq. 64)

η = transpiration coefficient = $0.60\ (29/M)^{0.26}$

θ = trajectory angle above horizon of sphere of radius $y + r_o$

$\bar{\theta}$ = angle around cylinder, reckoned so that $\bar{\theta} = 0$ at stagnation point in the cross-flow position

θ_E = initial re-entry angle

λ = proportionality constant for linear hydrogen loss rate (min^{-1})

μ = viscosity of air

μ_e = local viscosity of air at outer edge of boundary layer

μ^* = viscosity of air calculated at the reference enthalpy (see eq. 33)

μ_∞ = free stream viscosity of air (see eq. 31)

ρ = density of air (slugs/ft^3)

ρ_e = local density of air at the outer edge of the boundary layer (slugs/ft^3)

ρ_m = density of fuel rod material (slugs/ft^3)

$\rho_o\alpha$ = sea level density of air (slugs/ft^3)

ρ_s = stagnation point density (slugs/ft^3)

ρ_∞ = free stream air density (slugs/ft^3)

ρ^* = density evaluated at the reference enthalpy (slugs/ft^3)

σ = Stefan-Boltzman constant (Btu/ft^2-sec-$^\circ$R^4)

ϕ = pitch angle (angle cylindrical axis makes with direction of flow, $\phi = 0$ in end-on flow condition)

ω = angular velocity (radians/second)

Company Identification by Letters

AI — Atomics International (Division of North American Aviation, Inc.)

ARF — Armour Research Foundation, presently known as Illinois Institute of Technology Research Institute

CAL — Cornell Aeronautical Laboratories

GTC — General Technologies Corporation

IITRI — Illinois Institute of Technology Research Institute

NAAI — North American Aviation, Incorporated

SRI — Stanford Research Institute

I. INTRODUCTION

One of the problems attendant with the use of fuel-rod-carrying nuclear reactors in satellite applications is the possibility that these fuel rods will re-enter the earth's atmosphere without burning up entirely and reach the earth wholly or partially intact, thereby producing radiation hazards in populated areas. The purpose of the present program is to establish a mathematical model whereby various fuel element re-entry conditions can be simulated on a computer to determine if such fuel elements will indeed burn up at sufficiently high altitudes to render earth surface level hazards negligible.

Several previous studies on the fuel element materials have been made, as is evident from the bibliography in this report. These data, together with samples of fuel element material that had been subjected to simulated re-entry tests, formed the basis of the present study.

The problem of describing the re-entry behavior of nuclear fuel material may be divided into three general areas:

(1) Establishing the system of re-entry equations;

(2) Delineating the parameters that must be known in order to solve this system of equations; and

(3) Through chemical analysis on the samples and mathematical analysis of the available data, determining the values of these parameters. Those parameters that are not constant throughout the re-entry regime must be described in analytical form for simultaneous solution with the re-entry equations.

The system of equations has been established for the limited case of re-entry of cylindrical fuel rods, although the analysis may be applied to the more general case of re-entry of material of arbitrary shape. The assumptions used in deriving this system of equations

1

are: stationary planet atmosphere; planar trajectory; negligible effect of net lifting forces on the trajectory; and uniform wall temperature due to the rod spinning about its cylindrical axis. The parameters required for the solution of this set of simultaneous differential equations have been defined and their values determined as accurately as the existing data will allow.

The primary limitations on this study are due to the inadequacy of the available data. Some of those inadequacies are discussed at the end of the report and possible measures to overcome their shortcomings are suggested.

II. EQUATIONS OF MOTION AND RE-ENTRY

In this section, the trajectory and angular motion equations will be formulated together with the effects of ablation and accretion on these equations. The evaluation of the various parameters involved in these equations is the subject of the following section.

A. RE-ENTRY EQUATIONS

Five assumptions are employed in deriving the equations of motion of a re-entering vehicle. The first two of these are:

Assumption 1. The planet atmosphere is stationary.

Assumption 2. The re-entry trajectory is planar.

The following notation is employed:

r_o = radius of earth. (This can be considered as the distance from the center of gravity to the surface of a reference sphere having the average radius of the earth.)

y = altitude above earth's surface (can be considered as altitude above the surface of the reference sphere).

x = co-ordinate along the surface of a sphere from the point of re-entry, i.e., $(x,y) = (0, y_E)$ at the point of re-entry.

r = distance from center of gravity of vehicle to center of gravity of earth.

r_c = radius of curvature of trajectory.

θ = trajectory angle <u>above</u> horizon of sphere of radius $(r_o + y)$.

ds = distance along trajectory $(ds^2 = dy^2 + dx^2)$.

V = velocity of vehicle relative to stationary atmosphere.

ρ = density of atmosphere.

A = cross sectional area of vehicle (ℓd), ℓ = length, d = diameter of the vehicle.

3

W = weight of vehicle (at earth's surface), and

g = acceleration of gravity (at earth's surface), so that

W/g = mass of vehicle.

L_1 = lift of vehicle = $\frac{1}{2} \rho V^2 A C_L$.

C_L = lift coefficient.

D = drag of vehicle = $\frac{1}{2} \rho V^2 A C_D$.

C_D = drag coefficient.

t = time (taken as zero at point of re-entry, i.e. $(x, y, t) = (0, y_E, 0)$ at point of re-entry). E is a subscript denoting conditions at the point of re-entry.

Other symbols will be defined as they are brought into use.

Note that
$$\left.\frac{dy}{dx}\right|_E = -\tan \theta_E .$$

Now, it is appropriate to derive a relationship between r_o and r_c. To do this, refer to Figure 1. From the geometry, it follows that

$$ds = r_c \, d\gamma, \quad ds = r_o \sec \theta \, d\sigma, \quad \text{and} \quad -d\theta = d\gamma - d\sigma,$$

where $d\gamma$ is the elementary angle subtended by the elementary arc-length, ds, along the vehicle trajectory, and $d\sigma$ is the elementary angle subtended by ds, as viewed from a point at the center of gravity of the earth. Therefore,

$$-\frac{d\theta}{ds} = \frac{d\gamma}{ds} - \frac{d\sigma}{ds} = \frac{1}{r_c} - \frac{\cos \theta}{r_o} .$$

Thus, the following identities hold:

$$\frac{1}{r_c} = \frac{\cos \theta}{r_o} - \frac{d\theta}{ds} \approx \frac{1}{r_o} - \frac{d\theta}{ds} \quad \text{for small } \theta, \text{ and}$$

4
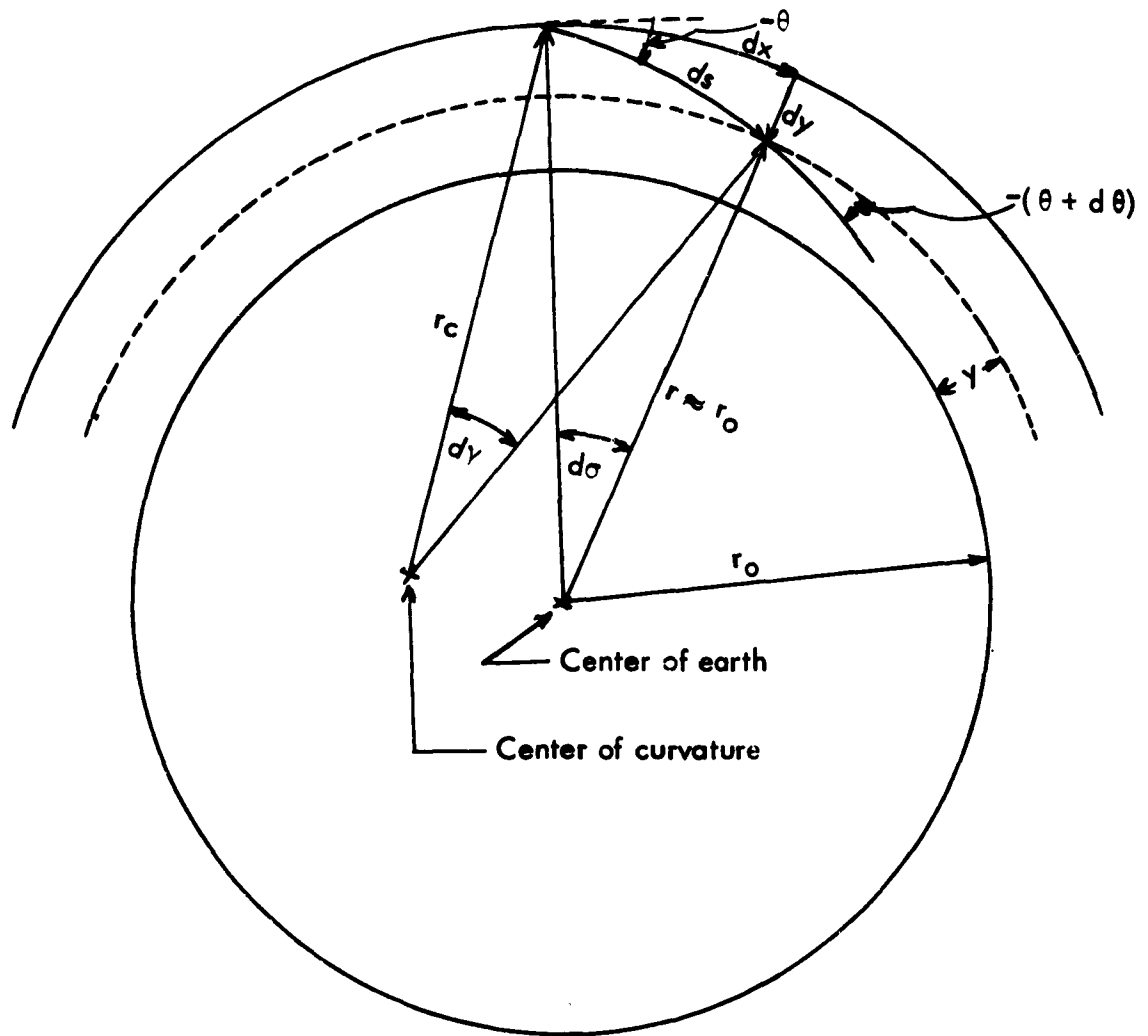
Figure 1. Diagram showing the relationship between coordinates and parameters at a point on a re-entry trajectory.

$$\frac{d\theta}{ds} = \frac{1}{V}\,\frac{d\theta}{dt}\,.$$

Hence,

$$\frac{1}{r_c} = \frac{\cos\theta}{r_o} - \frac{1}{V}\,\frac{d\theta}{dt}\,.$$

For forces normal to the flight trajectory, Figure 2 shows that

$$L_1 - W\left[\frac{r_o}{r}\right]^2 \cos\theta = -\frac{W}{g}\,\frac{V^2}{r_c}\,.$$

<u>Assumption 3.</u> Since the net effect of lift forces on the fuel element in question (a cylinder whose length is approximately ten times its diameter) only changes the length of the trajectory by a small fraction, they will be assumed to be negligible; hence,

$$-W\left[\frac{r_o}{r}\right]^2 \cos\theta = -\frac{WV^2}{g\,r_c} = -\frac{W}{g}\,V^2\left[\frac{\cos\theta}{r_o} - \frac{1}{V}\,\frac{d\theta}{dt}\right]$$

or

$$\frac{d\theta}{dt} = V\cos\theta\left[\frac{1}{r_o} - \frac{g\,r_o^2}{V^2 r^2}\right] \tag{1}$$

For forces along the flight path, Figure 2 shows that

$$D + W\left[\frac{r_o}{r}\right]^2 \sin\theta = -\frac{d}{dt}\left[\frac{W}{g}\,V\right].$$

Making use of the definition of the drag, D, and performing the indicated differentiation, this last expression becomes

$$\frac{1}{2}\rho V^2 A C_D + W\left[\frac{r_o}{r}\right]^2 \sin\theta = -\frac{V}{g}\,\frac{dW}{dt} - \frac{W}{g}\,\frac{dV}{dt}\,. \tag{2}$$

By definition of coordinates and θ, it follows that

$$\frac{dx}{dt} = V\cos\theta \tag{3}$$

$$\frac{dy}{dt} = V\sin\theta\,. \tag{4}$$

6
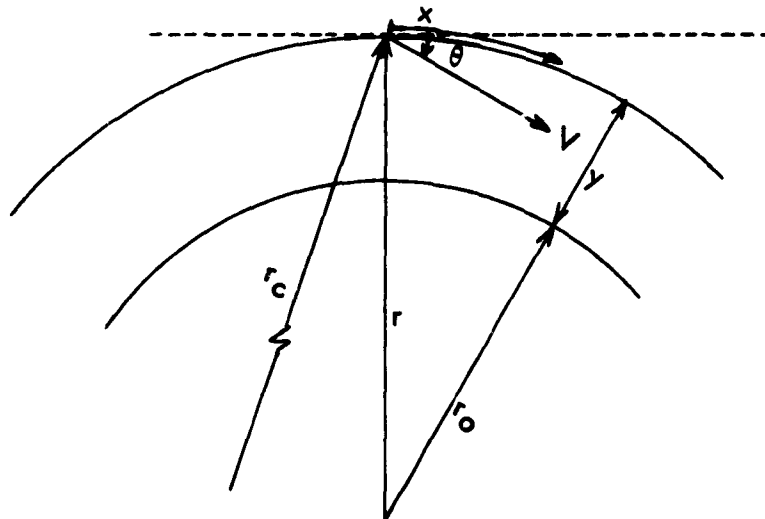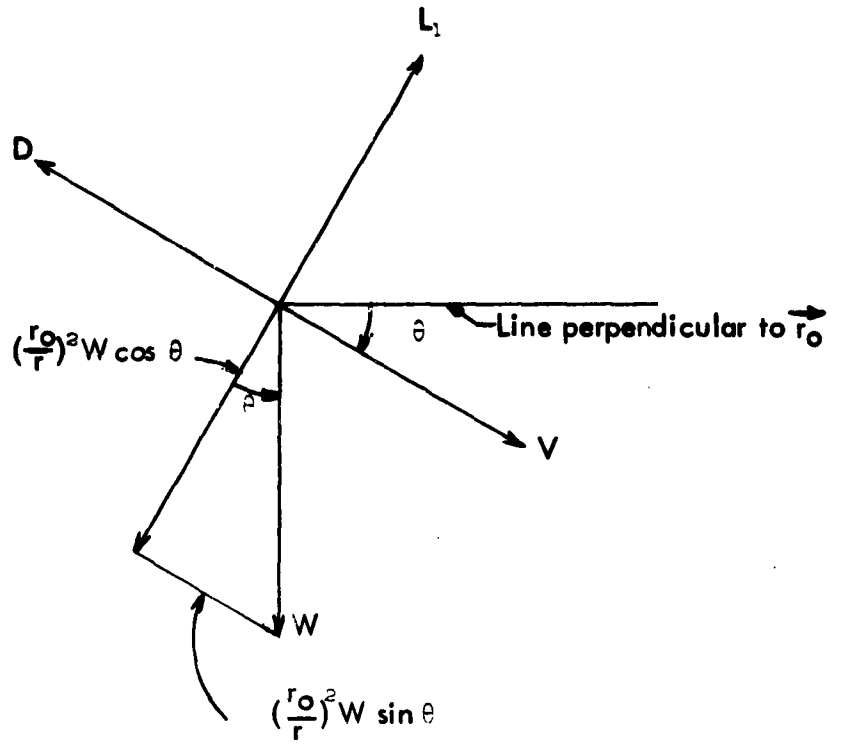
Figure 2. Diagrams showing the relationships between coordinates and vectors.

Figure 2. Diagrams showing the relationships between coordinates and vectors.

7
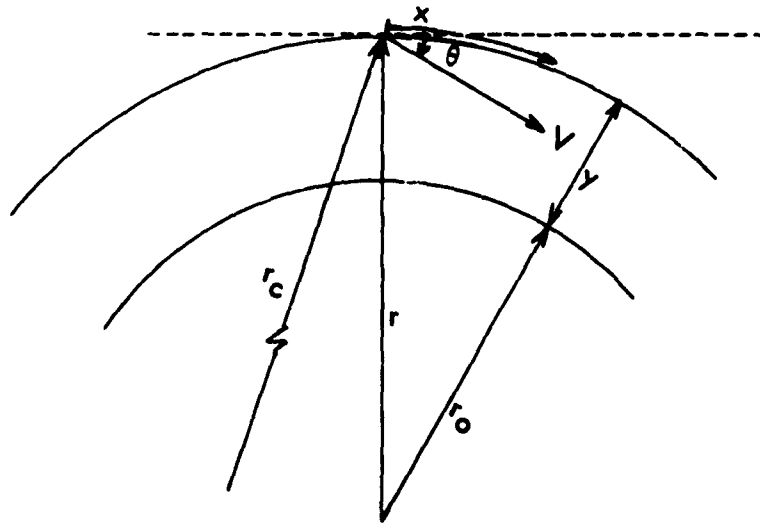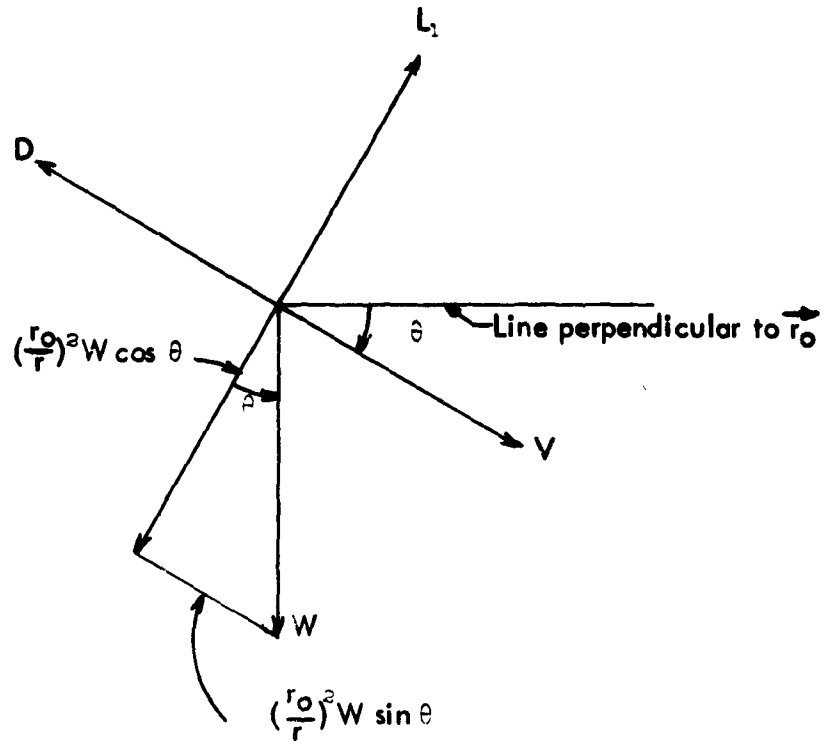
These four equations (eqs. 1, 2, 3, and 4) specify the re-entry motion of the fuel elements in terms of the initial conditions and

$$\frac{d\theta}{dt}, \frac{dV}{dt}, \frac{dx}{dt}, \frac{dy}{dt} \; .$$

The quantities V, r, W, and θ can be calculated from the foregoing equations if the quantities ρ, C_D, A, and dW/dt can be specified independently.

The value of ρ can be determined either from atmospheric tables or from the approximation:

$$\rho = \alpha \rho_o e^{-\beta y}$$

where

$\alpha \rho_o$ = sea level density (slugs/ft^3),

α = 0.715, and

β = 1/(24,800 ft).

The values of A and C_D must be determined from the angular motion of the rod, since they depend on the orientation of the fuel element for their specific values during any instant of time (t, t + dt). The dynamics of a re-entering rod are fairly well understood. (See, for example: Raymond and Garber,[1] Davey and Grigsby,[2] and others.)

B. ANGULAR MOTION EQUATIONS

The general angular motion (for a rod tumbling in the plane of the trajectory) should be governed by an equation of the form[9] *

$$\frac{d}{dt}(I\omega) = F(\phi, A, d, \rho_\infty, V_\infty), \tag{6a}$$

$$\omega = \frac{d\phi}{dt}, \tag{6b}$$

---

*Raymond assumes the static restoring and damping forces are respectively proportional to sin 2ϕ and cos$^2\phi$. AVCO's calculation[3] indicates that this is not far from correct.

8

where:

F = is a function to be defined in eq. (8).

∞ = subscript denoting free stream conditions.

ω = angular velocity of rod.

ϕ = angle of cylindrical axis of rod with respect to end-flow position.
($\phi = \pi/2$ at cross-flow; $\phi = 0$ for end-on flow condition.) ϕ is termed the pitch angle.

$I = \dfrac{W}{g} r_g^2$ = moment of inertia, with r_g = radius of gyration.

ℓ = length of rod   (feet).

d = diameter of rod   (feet).

$A = \ell d$.

ρ_∞ = free stream density (slugs/ft^3).

Performing the indicated differentiation in eq. (6a), making use of eq. (6c), and substituting an analytical fit to AVCO's[3] calculations on the static restoring and damping coefficients for F, the angular equation of motion becomes*

$$\frac{r_g^2}{g}\left[\omega\frac{dW}{dt}+W\frac{d\omega}{dt}\right] = 1.4\,\rho_\infty V_\infty^2\,A\,d\sin 2\phi\left[1+2.17\sin^2 2\phi\right] - 71\,\rho_\infty V_\infty A\,d^2\left|\sin\phi\right|. \quad (7)$$

Assumption 4. It has been assumed that r_g is constant in deriving eq. (7). When weight losses and/or dimensional changes are such that r_g cannot be considered constant, the term $(2\omega W r_g/g)\,d\,r_g/dt$ must be added to the left-hand side of eq. (7).

The two additional parameters $d\omega/dt$ and $d\phi/dt$, introduced by eq. (7), can be determined by the simultaneous solution of equations (6b) and (7) with equations (1) through (5), provided that the initial conditions on ϕ and ω are specified. Due to the relatively small

*Note, AVCO's curve (Fig. B-1-8 in ref. 3) could be read point for point into a computer program and used in place of the right-hand side of eq. (7). The overall accuracy of this analytical fit to AVCO's curve is within 5%.

thermal expansion of the fuel element material considered in this report, the effect of this expansion on r_g can be neglected for practical purposes. It should be emphasized that eq. (7) is valid only for cylindrical vehicles. If other vehicle shapes are to be used, the right-hand side of this relation has to be evaluated for the particular shape in question.

C. ABLATION EQUATIONS

In order to discuss accretion and ablation, it is necessary to consider the heat transfer to the rod, the temperature of the wall, etc. The quantity that can be discussed with the greatest degree of confidence is the rate of heat transfer to the fuel element.

Assumption 5. It is assumed that the fuel element will "spin" about its cylindrical axis so that the wall can be considered to be at a uniform temperature. Because of minor surface and/or internal irregularities, especially where tumbling is also taking place, this should be an accurate assumption up to the time large pieces of the rod have been ablated away. That is, fairly large asymmetries would be required to assure the stability of a cylinder during re-entry.

Assumption 6. It will be assumed, for the moment, that the fuel element remains at a uniform temperature throughout. This assumption will be examined in the next section, and a method for compensating for the fact that this assumption is not strictly correct will be presented.

With these assumptions, the instantaneous heat balance equation (in the absence of transpiration cooling or ablation) requires that

$$\frac{dT_w}{dt} = \left[C_H \, \rho_\infty V_\infty \, (h_e - h_w) + \dot{H}_{ch} - \varepsilon\sigma T_w^4 \right] \frac{S}{C_p} \frac{g}{W} \, . \tag{8}$$

where ρ, V, W, and g are as defined previously (∞ refers to free stream value).

10

T_w = temperature of wall ($^{\circ}$R).

C_H = average heat transfer coefficient (averaged over one cycle of "spin") — dimensionless.

h_e = stagnation enthalpy at outer edge of boundary layer (Btu/slug).

h_w = enthalpy of air at the wall temperature (Btu/slug).

ε = emittance of the wall material — dimensionless.

σ = Stefan-Boltzmann constant = 4.8×10^{-13} Btu/ft^2-sec$^{\circ}$R^4.

H_{ch} = rate of chemical heat input to rod due to chemical reactions (Btu/ft^3-sec).

S = surface area of rod (ft^2)

C_p = average specific heat capacity of rod (Btu/slug - $^{\circ}$R), and may be a function of its temperature history.

The heat transfer coefficient, C_H, which depends on the re-entry conditions and geometry of the vehicle in question, can be obtained from published literature, ostensibly from papers by: R. J. Vidal and C. E. Wittliff;[4] and J. C. Fay and F. R. Riddell.[5] The value of T_w is obtained from the initial conditions and eq. (8), solved simultaneously with the preceding seven equations. The emittance, ε, and the average heat capacity, C_p, must be known for every value of T_w. The quantity $\dot{H}_{ch}$ must be calculated from the environmental conditions and the chemical interaction of the rod material with the environment.

The change in weight rate, dW/dt, may be subdivided into three categories: the decrease in mass due to outgassing of the rod, the decrease in weight due to fusion (melting) and evaporation, and the increase in weight due to chemical interactions.

In the outgassing category (dehydriding), first assume that no outgassing takes place until a certain wall temperature, T_{wg}, is reached, and that $T_w = T_{wg}$ until all the gas has escaped. Then the heat balance equation for transpiration cooling requires that

$$-\frac{1}{g}\frac{dW}{dt}\bigg|_{deG,\,T_{wg}} = \frac{\left[C_H\,\rho_\infty V_\infty(h_e - h_{wg}) + \dot{H}_{ch} - \varepsilon\sigma T^4{}_{wg}\right]S}{H_{deG} + \eta(h_e - h_{wg}) - F_c H_{c,\,deG}} \qquad (9)$$

where

$\dfrac{1}{g}\dfrac{dW}{dt}\bigg|_{deG,\,T_{wg}}$ = rate of change in mass of the rod, in slugs/second, due to outgassing.

T_{wg} = the outgassing temperature.

H_{deG} = energy required to release one slug of gas (Btu/slug).

$H_{c,\,deG}$ = heat energy released in the combustion or re-combination of the transpired gas (Btu/slug).

η = transpiration coefficient (dimensionless).

F_c = fraction of the combustion energy, $H_{c,\,deG}$, that is absorbed by the fuel rod (dimensionless).

h_{wg} = enthalpy of air at the temperature T_{wg}.

Equation (9) neglects the rate of increase (or decrease) of weight due to $\dot{H}_{ch}$. This will be treated separately. The last term in the denominator of eq. (9) accounts for the effects due to possible changes in the state of an absorbed gas after it has been released from fuel rods such as the combustion or re-combination of the hydrogen as it is released. This relation is valid so long as the denominator is positive.

The value of η has been studied by Rose and Allenhartz[6] and by Georgiev.[7] It is given by

$$\eta = 0.60\left[\frac{29}{M_{deG}}\right]^{0.26}, \qquad (10)$$

where M_{deG} is the molecular weight of the outgassed material. This will be discussed in more detail in the following pages. In case more than one molecular weight is involved, M_{deG} is the average molecular weight, i.e., the weight, in grams, of a mole of the transpiring gas mixture.

In the case where the temperature does not remain constant during the blowing of the outgassing material, the situation becomes more awkward to treat mathematically. It can be handled in a formal manner when rod integrity (shape) is maintained. According to the theory of transpiration cooling,[6,7] the heat flux through the wall, $\dot{q}_{tr}$, with transpiration is less than the value, $\dot{q}_o$, without transpiration cooling by the factor $\eta(h_e - h_w)dm/dt$. The quantity dm/dt is just the rate of mass loss per unit area; hence,

$$\dot{q}_{tr} = \dot{q}_o - \eta(h_e - h_w)\left|\frac{1}{g}\frac{dW_1}{dt}\right|_{deG}$$

where $\left|\frac{1}{g}\frac{dW_1}{dt}\right|_{deG}$ is the magnitude of the weight loss rate per unit area due to the evolution of the transpiring gas. Now the heat balance condition requires that

$$\dot{q}_{tr} + \dot{H}_{ch} = (H_f + H_v)\left|\frac{1}{g}\frac{dW_1}{dt}\right|_{deG} + \frac{WC_p}{Sg}\frac{dT_w}{dt} + \varepsilon\sigma T_w^4.$$

Here, H_f and H_v are respectively the heats of fusion and vaporization of the material that is producing the evolving gas (Btu/slug). Eliminating $\dot{q}_{tr}$ from these two equations and noting that $\dot{q}_o = \rho_\infty V_\infty C_H(h_e - h_w)$, the expression for the rate of change in the total vehicle mass, due to transpiration, is

$$-\frac{1}{g}\frac{dW}{dt}\bigg]_{deG} = \frac{\left[\rho_\infty V_\infty C_H(h_e - h_w) + \dot{H}_{ch} - \varepsilon\sigma T_w^4 - \dfrac{WC_p}{gS}\dfrac{dT_w}{dt}\right]S}{H_v + H_f + \eta(h_e - h_w)}. \qquad (11)$$

This equation is to be used in place of eq. (9) when T_w is not constant during outgassing.

There may be an accretion of mass associated with the chemical reactions whose heat release (or absorption) rate is $\dot{H}_{ch}$. If M_r and M_{ch} are respectively the masses of the rod material and the accreted compound in slugs/gram-mole, then, clearly,*

$$\frac{1}{g}\frac{dW}{dt}\bigg]_{ch} = \left[\frac{\dot{H}_{ch}}{H_{ch}}\right](M_r - M_{ch})S, \qquad (12a)$$

*H_{ch} is negative for exothermic reactions, but $\dot{H}_{ch}$ always has the opposite sign of H_{ch}.

13

where H_{ch} is the heat of the reaction $M_r + O + N \longrightarrow M_{ch}$ in Btu/gram-mole. (The O and N may be molecular, partially ionized or atomic in this reaction.) If there are several reactions taking place, a summation over $\dot{H}_{ch}$, H_{ch}, and M_{ch} must be employed. When eq. (12a) is added to eq. (11), the net rate of mass loss (or gain) is obtained. These equations are valid so long as the accreted products remain on the rod. When (or if) the accreted products start to flake off of the rod, a different treatment is required.

In view of the fact that both $\left.\dfrac{dW}{dt}\right|_{deG}$ and $\dfrac{dT_w}{dt}$ appear in eq. (11), an equation similar to eq. (12a) must be deduced for separating these two parameters. For the present, this independent relationship will be written as

$$-\frac{1}{g} \left.\frac{dW}{dt}\right|_{deG} = G(T_w) \tag{12b}$$

Finally, the case of fusion and evaporation of the rod will be considered. This process is considered to take place at the fusion temperature, T_{wf}, and a certain fraction, F_v, of the material is assumed to evaporate and produce transpiration cooling. By similarity with eq. (9), this vehicle mass change rate is obviously given by

$$-\frac{1}{g} \left.\frac{dW}{dt}\right|_{vap-T_{wf}} = \frac{\left[C_H \, \rho_\infty V_\infty (h_e - h_{wf}) + \dot{H}_{ch} - \varepsilon\sigma T_{wf}^4\right] S}{H_f + F_v\left[H_v + \eta(h_e - h_{wf})\right]} \; . \tag{13}$$

It should be noted that eqs. (11) and (12) are to be solved simultaneously with eqs. (1) through (8). In a case where eqs. (9) and (13) are applicable, the first eight equations are followed until the respective wall temperatures reach T_{wg} and T_{wf}, and the temperature is then held constant (at T_{wg} or T_{wf}) until the process is completed. The use of eqs. (8) through (13) requires a knowledge of C_p, $\dot{H}_{ch}$, H_{ch}, M_{deG}, M_{ch}, H_v, H_f, T_{wg}, and T_{wf}.

14

III. EVALUATION OF PARAMETERS

The foregoing equations are sufficient to accurately describe the re-entry behavior of the fuel rod up to the point where the rod starts to break apart. They are still valid after the break-up begins, provided the various parameters associated with the imperfectly shaped remnants of the rod can be calculated or otherwise evaluated. The Assumptions 1 through 5 are, to within the present state of the art, quite satisfactory. Consequently, the only items that require a detailed analysis are:

$$C_D, C_H, C_p,$$

$$H_{c,deG}, H_{deG}, \dot{H}_{ch}, H_{ch}, H_f, H_v,$$

$$T_w, T_{wg}, T_{wf}, \epsilon, G(T_w),$$

$$M_{deG}, M_r, M_{ch}, F_c, F_v, \text{ and}$$

Assumption 6.

It is not necessarily true that all of these parameters will be required in a particular re-entry computation since the phenomena are, in some ways, related and may interfere with one another. For example, the formation of an oxide layer on the surface of the rod may prevent the transpiration of the hydrogen. Each of these parameters will now be analyzed.

A. VALIDITY OF ASSUMPTION 6, AND DETERMINATION OF C_p AND T_w

It will now be shown that Assumption 6 is quite convenient and permits one to write the equations of heating (eqs. 9, 11, 12, and 13) in forms which are readily manageable. By writing T_w and C_p in functional forms, the need for assuming a uniform temperature throughout the rod can be circumvented, as will be shown presently.

1. Temperature of the Rod

It will first be shown that the transient portion of the heat wave in the rod can be neglected to within certain limitations. Now, the major point of concern is the temperature difference between the surface and center of the rod. Since this difference, in an infinitely long rod, will be greater than or equal to the difference for a finite rod, an upper bound is obtained by considering an infinitely long rod. According to Carslaw and Jaeger,[8] the temperature at a distance $\bar{x}$ from the center of a circular cylinder of infinite length, for $\dot{q}_1 = $ constant, is given by

$$T(\bar{x}, t) = T_0 + \frac{4\,\dot{q}_1 t}{\rho_m C_p d} + \frac{\dot{q}_1 d}{2 k_m} \left\{ \frac{2\bar{x}^2}{d^2} - \frac{1}{4} - 2\sum_{n=1}^{\infty} e^{-\frac{4 k_m b_n^2 t}{\rho_m C_p d^2}} \left[\frac{J_0(2\bar{x} b_n / d)}{b_n^2 \, J_0(b_n)} \right] \right\} \qquad (14)$$

where T_0 is the initial uniform temperature of the rod at the time the heat flux $\dot{q}_1$ into the rod started to flow, J_n is the ordinary Bessel function of order n (J_0 being the zero-th order), and the b_n are the positive roots of

$$J_1(b) = 0. \qquad (15)$$

Here q_1 = normal heat flux into surface, and ρ_m, C_p, and k_m, are respectively the density, specific heat, and thermal conductivity of the rod. The quantity of interest is the temperature difference between the surface and center of the rod, namely,

$$T\left[\frac{d}{2}, t\right] - T(0, t) = \frac{\dot{q}_1 d}{2 k_m} \left\{ \frac{1}{2} + 2\sum_{n=1}^{\infty} \left[\frac{1}{b_n^2 \, J_0(b_n)} - \frac{1}{b_n^2} \right] e^{-\frac{4 k_m b_n^2 t}{\rho_m C_p d^2}} \right\} \qquad (16)$$

The exponential damping term assures that the transient portion of the temperature difference is rapidly damped out. The first four terms of the series are tabulated as follows:

n	b_n	$b_n^2 J_0(b_n)$	$\left[\dfrac{1}{b_n^2 J_0(b_n)} - \dfrac{1}{b_n^2}\right]$	$2\left[\dfrac{1}{b_n^2 J_0(b_n)} - \dfrac{1}{b_n^2}\right] e^{-\frac{4k_m b_n^2 t}{\rho_m C_p d^2}}$
1	3.832	-5.906	-.758	$-1.516 \exp\left[-2.45\,t\right]$
2	7.016	+14.77	+.047	$+.094 \exp\left[-8.22\,t\right]$
3	10.173	-25.81	-.0484	$-.0968 \exp\left[-17.28\,t\right]$
4	13.324	+38.72	+.0206	$+.0412 \exp\left[-29.65\,t\right]$

where

$$d^2 = .011\,ft^2,\quad k_m \approx .007\ Btu/ft\text{-}sec\text{-}^{\circ}R,^* \quad \rho_m \approx 380\ lbs/ft^3,\quad C_p \approx 0.1\ Btu/lb\text{-}^{\circ}R.$$

From this table, it is seen that

$$T\left[\frac{d}{2}, t\right] - T(0, t) = \frac{\dot{q}_1 d}{2 k_m}\left[\frac{1}{2} - 0.131\right] \text{ for } t = 1 \text{ second},$$

$$T\left[\frac{d}{2}, t\right] - T(0, t) = \frac{\dot{q}_1 d}{2 k_m}\left[\frac{1}{2} - 0.011\right] \text{ for } t = 2 \text{ seconds},$$

and

$$T\left[\frac{d}{2}, t\right] - T(0, t) = \frac{\dot{q}_1 d}{2 k_m}\left[\frac{1}{2} - 0.001\right] \text{ for } t = 3 \text{ seconds}.$$

From this it is apparent that the temperature difference is a minimum at the time $\dot{q}_1$ is "turned on" and reaches an approximately equilibrium value in a few (say 3) seconds. It is quite important to the present problem that the transient temperature effect dies out quickly. For high altitude fuel element release (> 250,000 ft.), no large changes in $\dot{q}_1$ over a period of three seconds or less will be experienced by the re-entering rod.[12] It is apparent from the above tabulation that the temperature difference between the surface and center of the rod is given, for practical purposes, by

$$T\left[\frac{d}{2}\right] - T(0) = \frac{\dot{q}_1 d}{2 k_m} \approx 7.4\ \dot{q}_1\ ^{\circ}R \tag{17}$$

*Actually, k_m varies from about 0.005 Btu/ft-sec-$^{\circ}R$ at 830$^{\circ}R$ to .009 Btu/ft-sec-$^{\circ}R$ at 3170$^{\circ}R$ according to ARF data.

17

where $\dot{q}_1$ is the net heat flux (Btu/ft²-sec) into the sample, that is, $\dot{q}_1 = C_H(h_e - h_w)\rho_\infty V_\infty + \dot{H}_{ch} - \epsilon \sigma T_w^4$ averaged over the surface of the rod.

In view of eq. (17) and the fact that $\dot{q}_1$ is not expected to exceed about 100 Btu/ft²-sec for fuel rod release altitudes of 250,000 ft. or greater, even with chemical reactions, it is reasonable to assume that the temperature variation within the rod will not exceed 740°R. At higher temperatures (where k_m is larger than .007), this temperature difference will be less. It will be shown in the following treatment of T_w that either considerably shorter time increments than three seconds or greater average heat fluxes than 100 Btu/ft²-sec will not introduce excessive errors in the calculation of T_w.

2. Determination of T_w

In order to use eq. (14) with varying $\dot{q}_1$, some means must be devised for accounting for the temperature distribution at the beginning of each time increment. In view of the fact that the transient part of eq. (14) will die out in three seconds, it is convenient to divide the heat flux pulse into a series of consecutive heat pulses, $\dot{q}_{1i}$, which appear as inputs to the fuel element at successive intervals that are three seconds or greater apart. Thus, in accordance with eq. (14), the wall temperature during the first time interval, (Δt_0), is

$$T_w(\Delta t_0) = T_0 + \frac{4\dot{q}_{10}\Delta t_0}{\rho_m C_p d} + \frac{\dot{q}_{10}d}{8k_m} . \qquad (18)$$

Note that Δt_0 can be varied continuously from three seconds onward but should be set at three seconds up to the time $\Delta t_0 = 3$ seconds in calculating T_w during the first three seconds. After the time Δt_0 has elapsed, a new heat flux pulse $\dot{q}_{11}$ replaces $\dot{q}_{10}$. This second heat pulse sees a different value of the rod temperature than the original T_0. The average increase in temperature of the rod during the first heat pulse is obtained from the enthalpy of the rod at the end of this pulse. If it is assumed that the heat capacity of the rod remains constant over the

18

temperature range present in the rod, the enthalpy of the rod is

$$(h_{rod})_{total} = 2\pi \, \rho_m C_p \ell \cdot \int_o^{d/2} \bar{x} \, T(\bar{x}) \, d\bar{x} .$$

Substituting eq. (14) for $T(\dot{x})$ into this expression, holding t and C_p constant, and integrating gives,

$$(h_{rod}) total = \frac{\pi d^2}{4} \, \rho_m \ell C_p T_o + \pi d \ell \, \dot{q}_1 t = (h_{rod})_o + \Delta h_{rod} ,$$

where Δh_{rod} is the increase in rod enthalpy due to the input $\dot{q}_1$ for the time t. Since $(h_{rod})_{total} = \rho_m \bar{C}_p \bar{T} \frac{\pi d^2 \ell}{4}$, in terms of the average rod temperature, $\bar{T}$, and average specific heat capacity, $\bar{C}_p$, it follows that the average temperature of the rod at the end of the first time interval, Δt_o, is

$$\bar{T}_1 = T_o + \frac{4 \dot{q}_{10} \Delta t_o}{\rho_m \bar{C}_p d} .$$

The value of $\bar{T}_{s+1}$ can be written immediately as

$$\bar{T}_{s+1} = T_o + \frac{4}{\rho_m \bar{C}_p d} \sum_{i=0}^{s} \dot{q}_{1i} \, \Delta t_i . \tag{19}$$

Here $\bar{T}_{s+1}$ is the average temperature of the rod, based on constant $\bar{C}_p$, at the beginning of the time interval Δt_s. Equation (18) may also be written in general form as

$$T_w(\Delta t_s) = \bar{T}_{s+1} + \frac{4 \dot{q}_{1s} \Delta t_s}{\rho_m \bar{C}_p d} + \frac{\dot{q}_{1s} d}{8 \, k_m} . \tag{20}$$

Now, it must be noted that C_p varies with temperature. To take this into account, it must be considered in calculating $\bar{T}_{s+1}$. The value of C_p at a particular temperature can be written as $B_1 + B_2 T$. If this functional form is substituted into eq. (20), the result is

$$T_w(\Delta t_s) = \bar{T}_{s+1} + \frac{\dot{q}_{1s} d}{8 \, k_m} + \frac{4 \dot{q}_{1s} \Delta t_s}{\rho_m (B_1 + B_2 T_{s+1}) d} \tag{21}$$

19

The appropriate value of $\overline{T}_{s+1}$ for use in eq. (21) is obtained by substitution of $B_1 + B_2 T_{s+1}$ into eq. (19) and solving for $\overline{T}_{s+1}$. The result is

$$\overline{T}_{s+1} = \frac{1}{2} \left[T_0 - \frac{B_1}{B_2} \right] + \frac{1}{2} \sqrt{\left[\frac{B_1}{B_2} + T_0 \right]^2 + \frac{16}{\rho_m B_2 d} \sum_{i=0}^{s} \dot{q}_{1i} \Delta t_i} \ . \tag{22}$$

When this value of $\overline{T}_{s+1}$ is substituted into eq. (21), the wall temperature is given. This value of T_w is used in equations (8) and (11). It is apparent from eq. (22) that the last time increment in the series (Δt_s) has a very small effect upon $\overline{T}_{s+1}$, or on $T_w(\Delta t_s)$, provided that s is large (say 10 or more).

3. Determination of C_p, B_1 and B_2

In accordance with the averaging process represented by eq. (22), it is clear that the effective value of C_p is

$$\overline{C}_p = B_1 + B_2 \overline{T}_{s+1} \ . \tag{23}$$

This is valid providing that Δt_s is kept sufficiently small and that the average value of C_p can be considered constant during the time interval Δt_s. Now, it has been pointed out that the transient effect due to increasing $\dot{q}_1$ from $\dot{q}_{1(s-1)}$ to $\dot{q}_{1s}$ has a small effect on $\overline{T}_s$ for large values of s, that is, when the transient heat pulse is superimposed upon a high enthalpy rod, the transient part of the heat pulse only contributes a small amount to the total enthalpy. Consequently, one can use quite small values of Δt_s, certainly on the order of one second, for the large values of s near the peak heating portion of the trajectory.

Because of the large mass of the fuel element relative to the mass of the oxide formed thereon, the change in heat capacity due to the conversion of some of the fuel element to oxides and/or nitrides can be neglected to a good approximation. Hedge, et al[10] (ARF data)

give the values of C_p without the coating layer of ZrO_2 and/or ZrN, and Wicks and Block[30] give the heat capacities (as a function of temperature) for ZrO_2 and ZrN.

It should be noted that Hedge, et al,[10] found that during the oxidizing of a sample of the fuel element material at the temperature 1930°R, no hydrogen was released. It took the sample about 160 seconds to come to an essentially equilibrium temperature in this particular case. This indicates that the hydrogen does not evolve up to temperatures of 1930°R. Their data on the oxidation in a 10% air, 90% argon atmosphere at 3010°R clearly show an initial decrease in mass which is consistent with the loss of most of the hydrogen in the specimen. The sample reached equilibrium in about 70 seconds in this case, and the center temperature reached 1930°R in about 20 seconds. Samples of fuel element material were exposed to a simulated re-entry trajectory (by varying the rate of heat energy input simultaneously with atmospheric pressure) by Littman[31] at SRI (Stanford Research Institute). He observed that water vapor appeared during these tests. The GTC chemical and metallographical analyses of the SRI samples confirm the loss of hydrogen from the samples that underwent the simulated re-entry tests. Except for the very low heating trajectory (SRI Trajectory 1A) simulated by SRI, essentially all of the hydrogen escaped, and even on this low heating trajectory, about 75% of the hydrogen escaped. These data represent the only experimental data available with which to determine the rate at which the hydrogen escapes through the surface. Although ARF tried to establish the diffusion rate of hydrogen through an oxide coating on a sample specimen of fuel element material, the experiments failed because of loss of oxide through structural failures. This will be discussed in more detail in the next subsection under $G(T_w)$.

There are two ways of handling the specific heat capacity of the fuel element material. The oxides and/or nitrides, if shown to be significant, can be handled separately. The ARF data show that the heat capacity of the hydrided material is higher than that of the dehydrided

21

material at temperatures above about 700°R and equal to it at high temperatures (2040°R).

It is here assumed that no hydrogen is lost during re-entry at temperatures below 2040°R.

The above mentioned data, as well as the analytical evaluation of such data (see Appendix II)

support this position. Thus, at high temperatures, it can be shown from the ARF data that the

heat capacity of the dehydrided material is

$$C_p \Big|_{Zr:U} = 0.0433 + 1.33 \times 10^{-5} T \quad Btu/lb - °R \text{ for } T \geq 2040°R. \quad (24)$$

Hence, $B_1 = .0433$, and $B_2 = 1.33 \times 10^{-5}$ in this temperature range. This will be slightly in

error in the vicinity of the transition point (α to β phase at 2040°R) but will be accurate at

the high temperatures. Similarly, the heat capacity of the hydrided material is

$$C_p \Big|_{Zr:H:U} = 0.108 + 2.65 \times 10^{-5} T \quad Btu/lb - °R \text{ for } 700 < T < 2040°R. \quad (25)$$

Hence, $B_1 = 0.108$, and $B_2 = 2.65 \times 10^{-5}$ in this temperature range.

Since the value of C_p does not change markedly in going from eq. (24) to (25), it is a

fair approximation to use either of these values in eqs. (21) and (22). For temperature very near

to 2040°R, eq. (14) can be used to establish what portion of the fuel rod should be treated as

having a heat capacity given by eq. (24), with the remainder being treated as having a heat

capacity given by eq. (25).

B. DRAG COEFFICIENT AND VARIATION WITH ANGLE OF ATTACK

The drag of the fuel element rod can be calculated from the "modified" Newtonian

theory. For this calculation, it is convenient to break the total drag down into two parts; that

is, the part due to the radial cylindrical surface and the part due to the ends.

Raymond's drag curve[9] is of little value in the present application since the l/d ratio

is quite different from that for the fuel element rod. Fortunately, Penland[11] has the Newtonian

22

C_D curve for an infinite cylinder. This curve is plotted in Figure 3. For a finite cylinder with flat or hemispherical ends, the values must be modified to allow for the end effects. The local pressure on the end face of the rod, which is now treated as a flat disc, is equal to $P_0' \cos^2\phi$, where P_0' is the normal shock recovery pressure. Thus, the normal force $= P_0' \cos^2\phi A_d$, where A_d is the area of the disc. The C_{Dd} for the disc, <u>based on the area of the disc</u>, is given by

$$C_{Dd} = \frac{P_0' \cos^2\phi \cos\phi A_d}{\frac{1}{2}\rho_\infty V_\infty^2 A_d} = \frac{P_0' \cos^3\phi}{\frac{1}{2}\rho_\infty V_\infty^2} \ .$$

Here $\frac{1}{2}\rho_\infty V_\infty^2$ is the free stream dynamic pressure. The drag coefficient, based on the <u>broad-side area A</u> of the cylinder is given by the relation

$$C_{Dd} = \frac{P_0' \cos^3\phi A_d}{\frac{1}{2}\rho_\infty V_\infty^2 A} \ ,$$

$$C_{Dd} = \frac{P_0' \cos^3\phi}{\frac{1}{2}\rho_\infty V_\infty^2} \ \frac{\pi}{4} \frac{d}{\ell} \ ,$$

$$C_{Dd} = \frac{\pi}{4} \times \frac{1.29\, P_\infty M_\infty^2}{\frac{\gamma}{2} P_\infty M_\infty^2} \cos^3\phi \ \frac{d}{\ell} \ ,$$

$$C_{Dd} = .146 \cos^3\phi \ ,$$

where $\frac{d}{\ell} = \frac{1}{10}$.

Table 1 shows how the total drag coefficient depends on the pitch angle, ϕ. The drag coefficient for the end disc is also plotted in Figure 3. Finally, the total drag coefficient is shown in Figure 3. A good analytical fit to this total drag curve is given by the following expression:

$$C_{D\,total} = .146 \cos^3\phi + 1.2 \sin^2\phi - .175 \sin^2(2\phi). \tag{26}$$

This function is tabulated in Table 2 and plotted in Figure 3.
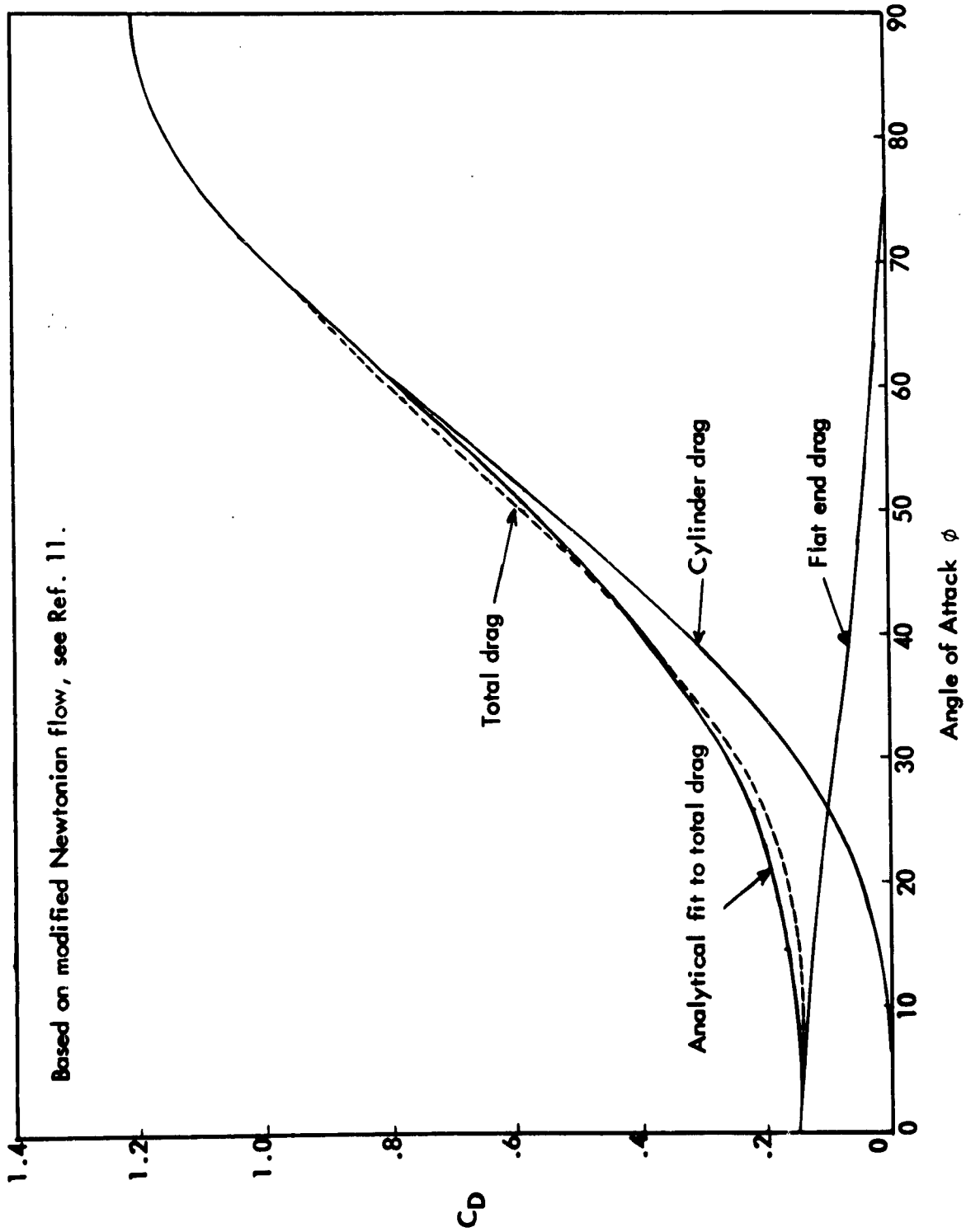
Figure 3. Cylinder Drag Coefficient

Table 1. Components and Total Drag Coefficients of a Cylinder with $l/d = 10$

ϕ	$\cos\phi$	$\cos^3\phi$	C_D Disc	C_D Cylinder	C_D Total
0°	1	1	.146	0	.146
10	.9848	.94	.137	.01	.147
20	.9397	.82	.120	.05	.170
30	.8660	.643	.0938	.155	.249
40	.7660	.446	.0652	.34	.41
50	.6428	.263	.0384	.54	.58
60	.5000	.125	.0183	.78	.80
70	.3420	.0400	.00584	1.0	1.0
80	.1736	.0052	.00076	1.15	1.15
90	0	0	0	1.2	1.2

Table 2. Tabulation of Equation 26

ϕ	$.146\cos^3\phi$	$1.2\sin^2\phi$	$.175\sin^2(2\phi)$	C_D Total
0	.146	0	0	.146
10	.137	.036	.0205	.1525
20	.120	.14	.0723	.1877
30	.0938	.30	.131	.2628
40	.0652	.496	.169	.3922
50	.0384	.704	.169	.5734
60	.0183	.90	.131	.7873
70	.00584	1.058	.0723	.992
80	.00076	1.16	.0205	1.14
90	0	1.20	0	1.20

If the rod has hemispherical ends, then the ends have a constant drag coefficient. At hypersonic speeds, this value, according to Kuehn,[48] is $C_D = 0.94$ if based on cross sectional area of the sphere. It should be noted that if the cylinder broadside area is used, then a different area from that used in the last analysis should be selected. The new area would simply be $(l - d)d + \dfrac{\pi d^2}{4}$. The drag coefficient for this case is obtained by multiplying numbers in the fifth column of Table 1 by the ratio $\left[(l - d)d + \dfrac{\pi d^2}{4}\right]\Big/ ld$. This modifies eq. (26) to read

$$C_{D \text{ total}}\bigg|_{\substack{\text{spherical} \\ \text{caps}}} = 0.069 + 1.17 \sin^2 \phi - 0.171 \sin^2(2\phi). \qquad (27)$$

Thus, if or when the edges of the fuel element burn away, eq. (27) is more appropriate than eq. (26).

C. EVALUATION OF HEAT TRANSFER COEFFICIENT C_H

In the re-entry regime of interest for the fuel element rod (altitudes of 300,000 feet or less), the heat transfer can be considered to be due to laminar aerodynamic heating. The heat transfer coefficient for the "no-blowing" case can be derived from the report of Vidal and Wittliff.[4] The effects of blowing are then handled in accordance with eqs. (9) through (13). The empirical expressions derived closely approximate the experimental results obtained in the Cornell Aeronautical Laboratory's Six Foot Hypersonic Shock Tunnel. These tests were carried out at Mach number from 17.13 to 23.46 at stagnation temperatures varying from $1800^\circ K$ to $5100^\circ K$ for a wide range of Reynolds numbers. These Reynolds numbers cover those appropriate to the fuel element over the altitude range 150,000 feet to 300,000 feet. The experimental data include both the real gas effects and the hypersonic interaction effects which will be encountered by the re-entering fuel element. The chemical effects of reaction heating, transpiration cooling, etc., will have to be handled independently. The determination of the aerodynamic heating effects is established in the following six subparagraphs.

1. Definition of Heat Transfer Coefficient

The laminar heat transfer coefficient is defined as[13]

$$C_H(K^2, \phi, \bar{\theta}) = \frac{\dot{q}}{\rho_\infty V_\infty (h_s - h_w)}, \qquad (28)$$

26

This empirical expression was derived by fitting a cubic equation to the data. Equation (35) is quite valid in the range $0.1 \leq K^2 \leq 100$. It agrees with the viscous shock layer theory of Cheng as well as that of Cohen and Reshotko.[4]

It should be noted that for $K^2 < 0.1$, one gets into the transition and free molecular flow regimes, and eq. (35) is not applicable. Also, for very large values of K^2, eq. (35) fails. It is actually <u>theoretically</u> correct for the conditions: $T_s \gg T_w$, $Pr = 0.71$, and $\epsilon^* = 0.10$; where ϵ^* is the density ratio across the normal shock, and Pr is the Prandtl number. However, it does fit the experimental data quite well, as indicated by Figure 4.

3. Heat Transfer Distribution Around the Circumference of a Cylinder

In the following discussion, the position around the circumference of the rod will be designated by $\bar{\theta}$, with $\bar{\theta} = 0$ at the stagnation point for the rod in cross flow. The quantity $\dot{q}(\bar{\theta})$ will be used to denote the heat transfer rate to the cylindrical surface at the angle $\bar{\theta}$.

It should be pointed out that there are discrepancies between the various experimental values of the ratio of $\dot{q}(\bar{\theta})/\dot{q}_s$ for various large values of $\bar{\theta}$ and some discrepancies for various values of the pitch angles ϕ. However, it can be shown that the scatter in the experimental data on variations with ϕ are submerged in the effects of variations in the data on K^2. Consequently, one is justified in ignoring the effects of ϕ on $\dot{q}(\bar{\theta})$ until better experimental data become available. The arguments for using a single parameter function for $\dot{q}(\bar{\theta})/\dot{q}_s$ are as follows:

a. The laminar heat transfer distribution around the circumference of a cylinder re-entering with its cylindrical axis normal to the flow ($\phi = 90°$) is shown in Figure 5 (see also Figure 6, Ref. 4), and results for ϕ up to $45.5°$ are shown in Reference 4, Figure 8. The experimental values obtained by Vidal and Wittliff (for $M = 17 - 23$) are considerably lower

28
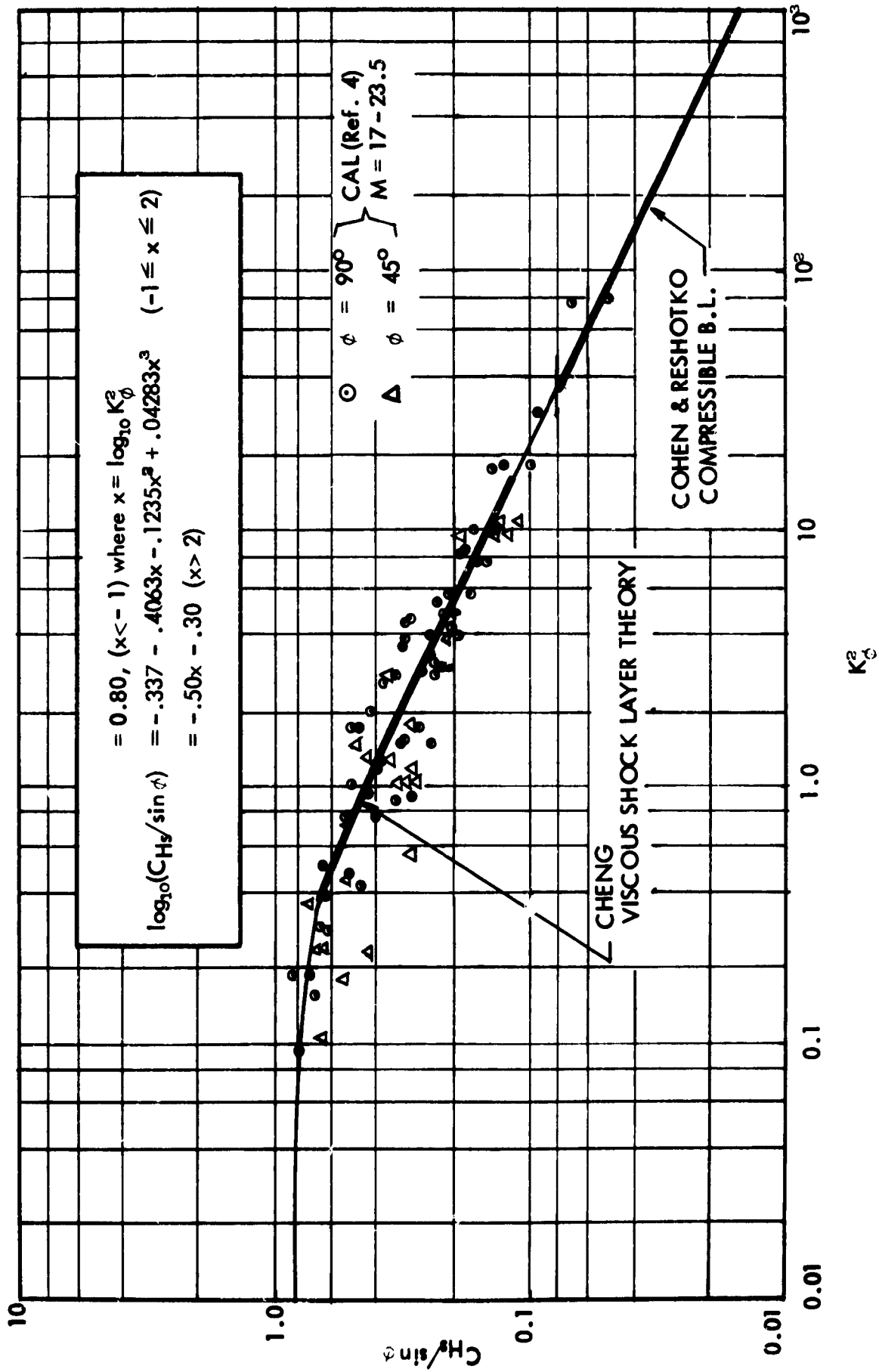
Figure 4. Heat transfer to a yawed cylinder.

The figure plots $\frac{\dot{q}(\bar{\theta})}{\dot{q}_s}$ versus $\bar{\theta}$ (Deg), with the following labels:

- Tewfik & Giedt $\phi = 90°$
- Beckwith $\phi = 90°$, $\phi = 30°$
- Experiment (CAL (Vidal & Wittliff) $0.8 < K^2 < 5$, $45° < \phi < 90°$

$$\log_{10}\left(\frac{\dot{q}}{\dot{q}_o}\right) = 3\left[\cos\frac{\bar{\theta}}{2} - 1\right]$$
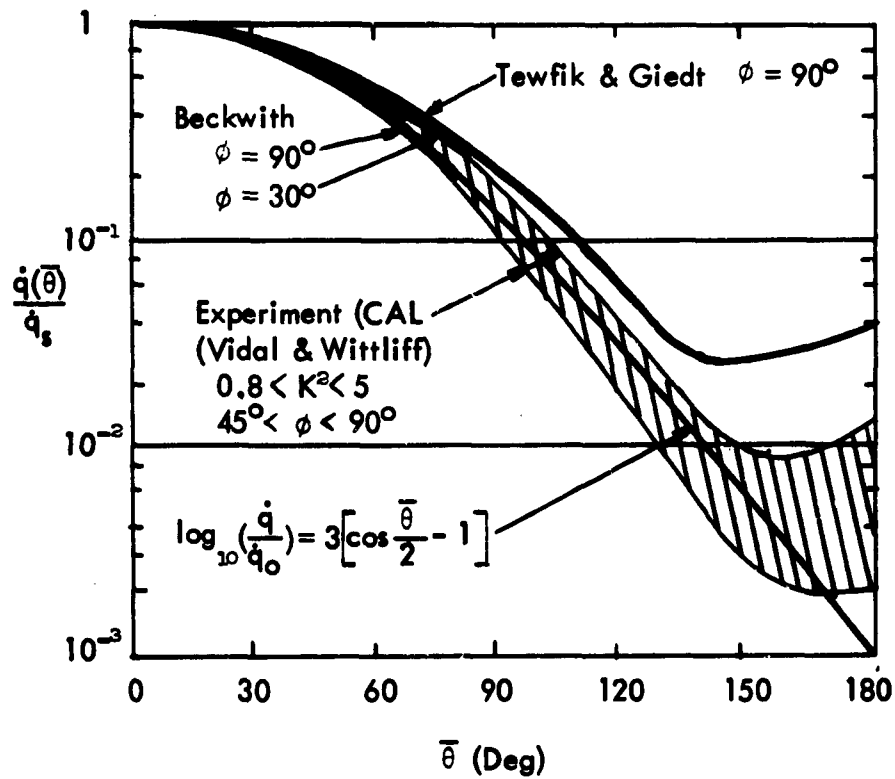
Figure 5. Circumferential heat transfer distribution on a yawed cylinder.

30

than those obtained by Tewfik and Giedt.[15] This is particularly true for the back side of the rod, i.e., for $90° < \bar{\theta} < 180°$.

b. For $0 < \bar{\theta} < 90°$, the Vidal and Wittliff data agree well with the theoretical distribution derived by Beckwith[16] for laminar boundary heating of a cylinder. (See Ref. 4 for detailed comparison.)

c. Laminar separation on the back side of the cylinder is evidenced by the dependence of $\dot{q}(\bar{\theta})$ on K^2 (see Fig. 5). That is, laminar separation is affected by the Reynolds number. Fortunately, the effect of laminar separation is only pronounced for $\bar{\theta} > 120°$ for which $\dot{q}(\bar{\theta})/\dot{q}_s < .03$, i.e., less than 3% of the stagnation value. Thus, one is justified in fitting an average curve through all of the experimental data points for various values of K^2.

d. Although the theory of Beckwith predicts a dependence of $\dot{q}(\bar{\theta})$ on ϕ, the data of Vidal and Wittliff (see Figure 5) shows that if there is such a dependence, it is submerged by the influence of laminar separation. The spread in data is represented by the fact that for $\phi = 90°$ and $45.5°$, observed values of $\dot{q}(\bar{\theta})/\dot{q}_s$ are essentially the same for values of $K^2 = 2$ and 5, whereas at $\phi = 60°$ and $K^2 = 1.6$, the observed value is quite different. Hence, it may be concluded that variations in $\dot{q}(\bar{\theta})/\dot{q}_s$ with ϕ are not justifiable on the basis of experimental data.

e. Finally, in view of arguments (c) and (d), it is concluded that a single parameter curve of $\dot{q}(\bar{\theta})/\dot{q}_s$ versus $\bar{\theta}$ is all that can be justifiably employed. A curve that fits the data presented by Vidal and Wittliff[4] is

$$\log_{10}\left[\dot{q}(\bar{\theta})/\dot{q}_s\right] = 3\left[\cos\frac{\bar{\theta}}{2} - 1\right] . \tag{36}$$

This relation is compared with the aforementioned experimental results in Fig. 5. It is seen that the empirical equation agrees quite well with the experimental data for the forward

31

portion of the fuel rod and is in fair agreement on the back side where the heat transfer is quite small compared to $\dot{q}_s$.

It will be assumed, as mentioned above, that the fuel rod will spin about its cylindrical axis, hence it is practical to use an average value, $\dot{q}_a$, for the heat flux. Rewriting eq. (36) in exponential form and integrating gives

$$\dot{q}_a = \frac{2\dot{q}_s}{\pi} \int_0^{\pi/2} \exp\left[6.9078 \,(\cos\alpha - 1)\right] d\alpha = 0.310 \,\dot{q}_s. \tag{37}$$

This integral was evaluated from Figure 6, which illustrates the variation of $\dot{q}$ with $\bar{\theta}$.

4. Heat Transfer Rate to a Pitching Cylinder

Now that the heat transfer at the stagnation point (eq. 35) and the effect of spin (eq. 37) on it have been developed in analytical form, there remains to be determined the effect of pitch angle on the heat transfer.

The experimental data on stagnation line heat transfer to yawed cylinders have been reviewed in Ref. 4 and presented in Figure 7 thereof. This data, together with the Vidal-Wittliff data was used to construct the curve shown in Figure 4. Theoretical solutions have been obtained by Cheng and Chang[17] which indicate $(C_{H_s})/\sin\phi$ is principally a function of $K^2(\phi)$, where

$$K^2(\phi) = \frac{Re_\infty}{\gamma_\infty M^2_\infty C^*(\phi) \left|\sin\phi\right|}. \tag{38}$$

Similarity with equations (31), (32), and (33) gives

$$C^*(\phi) = \frac{\mu^*(\phi) T_\infty}{\mu_\infty T^*(\phi)}, \tag{39}$$

$$T^*(\phi) = \frac{1}{2}(T_w + T_s \sin^2\phi), \tag{40}$$

32
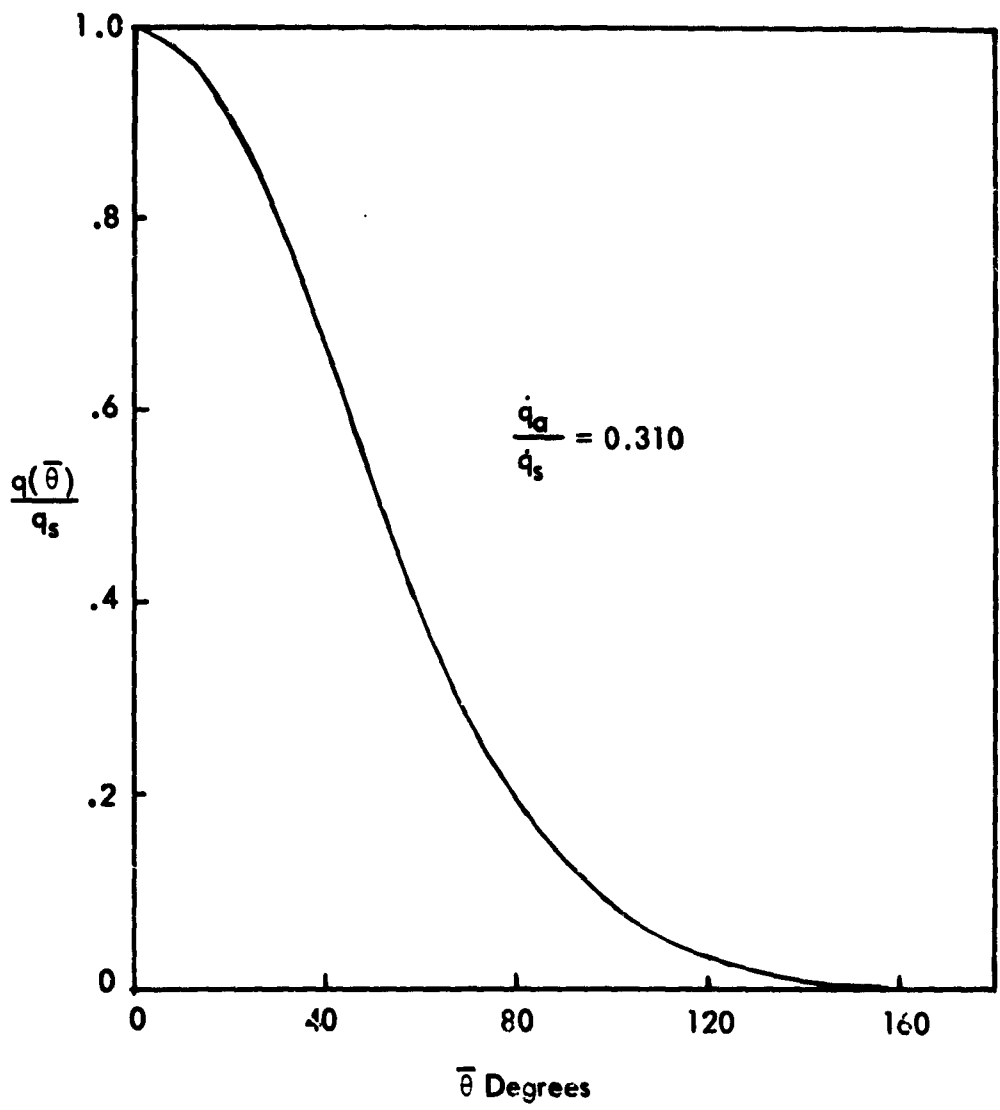
Figure 6. Variation of heat flux with $\overline{\theta}$.

The figure shows a plot with y-axis labeled $\frac{q(\overline{\theta})}{q_s}$ ranging from 0 to 1.0, and x-axis labeled $\overline{\theta}$ Degrees ranging from 0 to 160. The annotation reads $\frac{\dot{q}_a}{\dot{q}_s} = 0.310$.

33

and $\mu^*(\phi)$ is to be evaluated at the reference temperature, $T^*(\phi)$. The $\sin^2 \phi$ term arises from viscous shock wave theory.[17] In terms of more conventional parameters, eq. (38) may be written as

$$K^2(\phi) = \frac{\rho_\infty V_\infty d}{4 \gamma_\infty M_\infty^2 \mu^*(\phi)} \left[\frac{T_w + T_s \sin^2 \phi}{T_\infty |\sin \phi|} \right] \text{ for } 0.1 \leq K^2(\phi) \leq 100. \tag{41}$$

The absolute value is used on the $\sin \phi$ in order that ϕ may vary from 0 to 2π. The limits (0.1 to 100) for the range of $K^2(\phi)$ are in good agreement with the experimental data of Vidal and Wittliff. The curve must be extrapolated beyond the upper limit to $K^2(\phi) = 100$.

Although Cheng and Chang found that $C_{Hs}/\sin \phi$ is weakly dependent upon ϕ, both theory and the experimental results of Vidal and Wittliff indicate that it is small enough to be neglected. This is referred to as the "yaw – independence principle." In view of this principle, eq. (35) still holds when $K^2(\phi)$ and $C_{Hs}/\sin \phi$ are substituted for C_{Hs} and K^2, that is

$$\log_{10}(C_{Hs}/\sin \phi) = -.337 - .4063 \log_{10} K^2(\phi) - .1235 \left[\log_{10} K^2(\phi) \right]^2 + .04283 \left[\log_{10} K^2(\phi) \right]^3$$
$$\text{for } 0.1 \leq K^2(\phi) \leq 100 < \overline{K}^2(\phi). \tag{42}$$

For values of $K^2(\phi) > 100$, the following equation should be used.

$$\log_{10}(C_{Hs}/\sin \phi) = -0.5 \log K^2(\phi) - 0.30. \tag{43}$$

This equation is illustrated by the section of the curve in Figure 4 that lies between $K^2(\phi) = 100$ and 1000. For $K^2(\phi) < 0.1$, the value of C_{Hs} calculated at $K^2(\phi) = 0.1$ by eq. (42) should be used, i.e.,

$$C_{Hs}(K^2, \phi) = C_{Hs}(0.1, \phi). \tag{44}$$

Equation (44) is not needed for altitudes below 300,000 ft.

34

5. Heat Transfer to Afterbody

For values of $K^2(\phi)$ greater than some value $\overline{K}^2(\phi)$, C_{H_s} is equal to the afterbody heat transfer coefficient (neglecting ends of cylinder) of the cylinder in the end-on flow position. (The heat transfer to the ends of the cylinder will be treated in the following section.) This is a little more involved and requires some detailed discussion. Based on Blasius incompressible flow skin friction, modified for application to compressible flow by evaluating $\mu \rho$ at the reference enthalpy of Eckert,[18] together with Colburn's version of the Reynold's analogy,[19]

$$St = \frac{1}{2} \overline{C}_f \, Pr^{-2/3},$$

$$\dot{q}_{ab} = C_H \rho_e V_e (h_r - h_w). \tag{45}$$

Here $\dot{q}_{ab}$ = heat flux to afterbody,

μ = viscosity of air,

Pr = Prandtl number = $4\gamma/(9\gamma - 5)$,

C_f = local skin friction coefficient ($\overline{C}_f$ = mean value of C_f), and

h_r = recovery enthalpy (defined below).

The value of C_H is given by Hayes and Probstein as[19]

$$C_{H_{ab}} = \frac{0.664}{\sqrt{(Re)_\ell}} \, Pr^{-2/3} \sqrt{\frac{(\rho\mu)^*}{(\rho\mu)_e}}. \tag{46}$$

The asterisk refers to quantities evaluated at the reference enthalpy, the subscript e refers to local values at the outer edge of the boundary layer, and

$$(Re)_\ell = \frac{\rho_e V_e \ell}{\mu_e}. \tag{47}$$

The reference enthalpy of Eckert is used, i.e.,

$$h^* = \frac{1}{2}(h_e + h_w) + 0.22(h_r - h_e), \tag{48}$$

and

$$h_r = h_e + (h_s - h_e)\sqrt{Pr} . \tag{49}$$

Cohen[20] gives the value of $(\rho\mu)^*/(\rho\mu)_e$ as

$$\frac{(\rho\mu)^*}{(\rho\mu)_e} = \frac{1 - 1.0213\left[1 - (h_e/h')^{0.5329}\right]}{1 - 1.0213\left[1 - (h^*/h')^{0.3329}\right]} . \tag{50}$$

The value of h' is 272,234 Btu/slug (8465 Btu/lb).

Now the values of ρ_e, V_e, μ_e, and h_e (local flow on the afterbody) must be found. This can be accomplished as follows: For present purposes, perfect gas theory will be used,[21] and the pressure, P_s, behind the shock wave (edge of boundary layer in front of stagnation point) will be calculated from the Rayleigh-Pitot tube formula, which gives

$$\frac{P_s}{P_\infty} = \left[\frac{6}{5}M_\infty^2\right]^{7/2}\left[\frac{6}{7M_\infty^2 - 1}\right]^{5/2} . \tag{51}$$

The value of P_e, the local Pitot pressure at the outer edge of the boundary layer, can be determined from the graph presented by Chernyi,[22] which is based on hypersonic flow. An analytical fit to this graph is

$$\frac{P_e - \frac{1}{2}P_\infty}{\frac{1}{2}\rho_\infty V_\infty^2} = K'(\gamma)\sqrt{(d/x_e)C_D} . \tag{52}$$

Here x_e is the distance along the surface of the cylinder from the stagnation point. The quantity $K'(\gamma) = 0.095$ for $\gamma = 1.4$; $= 0.080$ for $\gamma = 1.2$; and $= 0.065$ for $\gamma = 1.1$. A reasonable approximation is to take $d/x_e = .2$ (the average value), $\gamma = 1.2$, and $C_D = 1.84$ (see ref. 43),

36

$$P_e = P_\infty + 2.02 \times 10^{-2} \rho_\infty V_\infty^2 . \tag{53a}$$

It should be mentioned that Kuehn [43] used $P_\infty/2$ in place of P_∞ in this last equation. For $M_\infty > 15$, this makes little difference. For smaller values of M_∞, one should use

$$P_e = \frac{1}{2} P_\infty + 2.02 \times 10^{-2} \rho_\infty V_\infty^2 . \tag{53b}$$

For an isentropic expansion of the Pitot pressure along the afterbody,

$$\frac{P_e}{P_s} = \left[1 + \frac{M_e^2}{5}\right]^{-7/2}, \text{ or } M_e = \left\{5\left[\frac{P_s}{P_e}\right]^{2/7} - 5\right\}^{1/2} . \tag{54}$$

The temperature, T_e, in terms of the temperature, T_s (at the edge of the boundary layer in front of the stagnation point), is given by

$$\frac{T_e}{T_s} = \left[1 + \frac{M_e^2}{5}\right]^{-1}, \text{ or } T_e = T_s\left[\frac{P_e}{P_s}\right]^{2/7} , \tag{55}$$

where $T_s = h_s/C_{pa}$, and C_{pa} is the specific heat capacity of air = 7.73 Btu/slug - $^\circ$R. The sound speed is a_e, and $V_e = a_e M_e$, where

$$a_e = \sqrt{\gamma R_g T_e} , \quad R_g = 1715 \text{ ft-lbs/slug} - ^\circ\text{R}. \tag{56}$$

Therefore, from the above relations, it is readily shown that

$$V_e = \sqrt{5 \gamma R_g (h_s C_{pa} - 1)} . \tag{57}$$

The density is $\rho_e = P_e/R_g T_e$, which, by the above formulas, is

$$\rho_e = \frac{6 M_\infty^2 P_\infty^{2/7}}{5 R_g h_s C_{pa}} \left[\frac{6 P_\infty + 0.126 \rho_\infty V_\infty^2}{7 M_\infty^2 - 1}\right]^{5/7} . \tag{58}$$

The viscosity, according to Sutherland's formula, becomes

37

$$\mu_e = 2.27 \times 10^{-8} \left\{ \frac{\left[\dfrac{5 h_s C_{pa}}{6 M_\infty^2}\right]^{3/2}\left[\dfrac{P_\infty + .021\, \rho_\infty V_\infty^2}{P_\infty}\right]^{3/7}\left[\dfrac{7 M_\infty^2 - 1}{6}\right]^{15/14}}{\dfrac{5 h_s C_{pa}}{6 M_\infty^2}\left[\dfrac{P_\infty + .021\, \rho_\infty V_\infty^2}{P_\infty}\right]^{2/7}\left[\dfrac{7 M_\infty^2 - 1}{6}\right]^{5/7} + 198.6} \right\}. \tag{59}$$

Here, the values of C and S* have been taken from Reference 21 (see eq. 33). The value of h_e is taken as $h_e = T_e C_{pa}$, that is

$$h_e = \frac{5 h_s C_{pa}^2}{6 M_\infty^2}\left[\frac{P_\infty + .021\, \rho_\infty V_\infty^2}{P_\infty}\right]^{3/7}\left[\frac{7 M_\infty^2 - 1}{6}\right]^{5/7}. \tag{60}$$

When equations (57) through (60) are substituted into (46) through (50), all of the parameters in eq. (45) are given in terms involving conditions in front of the shock wave and at the stagnation point enthalpy. This latter quantity is simply

$$h_s = \frac{V_\infty^2}{2J} = C_{pa} T_s . \tag{61}$$

Note, now, that C_{Hab} must be used in place of the value of C_{Hs}, as calculated from eq. (33), when the latter becomes small. That is, use C_{Hab} when

$$C_{Hab} \gtrsim 0.310\, C_{Hs} . \tag{62}$$

6. Heat Transfer to Ends of Cylinder

The heat transfer rate to the end face of a cylinder in end-on flow is nearly constant according to Kemp, Rose, and Detra (see Fig. 5 of Ref. 23). According to Detra and Hidalgo,[24] the heating rate is

$$\dot{q}_{end} = \frac{865}{(d/2)^{1/2}}\left[10^{-4} V_\infty\right]^{3.15}\left[\frac{\rho_\infty}{\alpha\, \rho_0}\right]\left[\frac{h_s - h_w}{h_s - h_{w300}}\right]\left[\frac{\zeta}{\zeta_n}\right]^{1/2} \quad \text{(end-on flow)}. \tag{63}$$

Here $\zeta = (du/dx)_s$ = stagnation point velocity gradient,

   ζ_n = Newtonian value of ζ, and

   h_{w300} = wall gas enthalpy at $T_w = 300°K$ (540°R), hence, $h_{w300} = C_{pa} T = 7.73 \times 540 = 4175$ Btu/slug.

This equation is accurate to within 10% for $6000 \leqslant V_\infty \leqslant 26,000$ ft/sec and for $8 \times 10^{-5} \leqslant \rho_\infty / \alpha \rho_0 \leqslant 1$.

$$\zeta_n = \frac{2}{d} \sqrt{\frac{2(P_s - \rho_\infty)}{\rho_s}} \approx \frac{2}{d} \sqrt{\frac{2P_s}{\rho_s}} = \frac{2}{d} V_\infty \sqrt{\frac{\gamma - 1}{\gamma}} \ . \tag{64}$$

For large values of M, Probstein[25] shows that the correct value of ζ is

$$\zeta = \frac{1.2}{d} V_\infty \sqrt{\frac{\gamma - 1}{\gamma + 1}} \ . \tag{65}$$

Hence,

$$\frac{\zeta}{\zeta_n} = 0.6 \sqrt{\frac{(\gamma - 1)\gamma}{\gamma^2 - 1}} \ . \tag{66}$$

Since the heat transfer rate is expected to be proportional to P_s, and the pressure distribution on the end of the cylinder varies as $\cos^2 \phi$ (see Weinstein[42] for experimental verification), the heating rate becomes, upon substitution of eqs. (64), (65), and (66) into (63),

$$\dot{q}(\phi)_{end} = 6.70 \times 10^{-10.6} \frac{\rho_\infty V_\infty^{3.15}}{\alpha \rho_0 \sqrt{d}} \left[\frac{h_s - h_w}{h_s - 4175} \right] \left[\frac{(\gamma - 1)\gamma}{\gamma^2 - 1} \right]^{1/4} \cos^2 \phi \ . \tag{67}$$

The appropriate values of γ have been tabulated by Wittliff and Curtis;[26] however, $\gamma = 1.2$ would not lead to gross error in the high heating part of the re-entry trajectory.

Summarizing, the values of C_H to be used in equations (8), (9), and (11) are:

a. $0.1 \leqslant K^2(\phi) \leqslant 100 < K'$.

Take the sum of the value obtained by using eq. (42) (multiplied by 0.310) and the value $\dot{q}_{end}(\phi)/\rho_\infty V_\infty (h_s - h_w)$, where $\dot{q}_{end}(\phi)$ is calculated from eq. (67).

b. $K^2(\phi) < 0.1$.

Take the value obtained when $K^2(\phi) = 0.1$ is substituted into eq. (42), multiply by 0.310, add the value of $\dot{q}_{end}(\phi)/\rho_\infty V_\infty (h_s - h_w)$ obtained from eq. (67).

c. $K^2(\phi) > 100$ and $C_{Hab} < 0.310\, C_{Hs}$.

Multiply the value of C_{Hs} obtained from eq. (43) by 0.310, and add it to $\dot{q}_{end}(\phi)/\rho_\infty V_\infty (h_s - h_w)$.

d. $C_{Hab} \gtrsim 0.310\, C_{Hs}$.

Take the value of C_{Hab} obtained from eq. (46) and add it to $\dot{q}_{end}(\phi)/\rho_\infty V_\infty (h_s - h_w)$.

D. EVALUATION OF ϵ

The data on the emittance from Hedge, et al can be represented to within about 1% by the equation

$$\epsilon = -0.08 + \frac{1}{2500} \sqrt{2 \times 10^6 + 3500\,T - T^2} \,. \tag{68}$$

E. EVALUATION OF H_{ch}, $\dot{H}_{ch}$, AND $\left.\dfrac{dW}{dt}\right|_{ch}$

In this category, there are three major considerations, that of the heat input due to the oxidation and/or nitridation of the fuel rod material, the rate of weight accretion due to these reactions, and the heat input (or loss) due to the dehydriding and combustion of hydrogen contained in the fuel element material. The available data have been analyzed in Appendix II.

1. Evaluation of $\left.\dfrac{dW}{dt}\right|_{ch}$

The data[10] on the oxidation and/or nitridation of the fuel element material shows that the weight gain rate during oxidation follows the parabolic law, except during dehydriding, within the accuracy of the experiments. (See Appendix II for a detailed analysis of the available data.) That is,

$$(\Delta m_s)^2 = k_s t \tag{69}$$

where Δm_s is the weight gain per unit area in a time t, and k_s is a temperature dependent parameter (reaction constant) which obeys the Arrhenius relation

$$k_s = A_s e^{-Q_s/T}. \tag{70}$$

The oxidation data of reference 10, after correcting for sample shape and size, are plotted in Figure 7. The straight line represents the parabolic curve, and the points represent the experimental data. The values of A_s and Q_s were determined by plotting $\log k$ versus $1/T$ as shown in Figure 8. This figure shows that the pre-factor, A_s, and the activation energy, Q_s (actually $R_g Q_s$), change at the phase change of the fuel material, i.e., at about $2040^\circ R$. For t in minutes and Δm_s in grams per square centimeter, the numerical values of A_s and Q_s are

$$A_s = 0.356 \text{ gm}^2/\text{cm}^4 - \text{min, and } Q_s = 2.59 \times 10^{4\circ}R \text{ for } T \leqslant 2040^\circ R, \tag{71a}$$

$$A_s = 92.5 \text{ gm}^2/\text{cm}^4 - \text{min, and } Q_s = 3.79 \times 10^{4\circ}R \text{ for } T \geqslant 2040^\circ R. \tag{71b}$$

To convert Δm_s to pounds per sq. ft., one first divides A_s by sixty to obtain $\text{grams}^2/\text{cm}^4 - \text{sec}$ and then multiplies by 2.04 to convert to $\text{lbs}^2/\text{ft}^4 - \text{sec}$. Thus, eq. (69) becomes

$$\Delta m_s = 3.4 \times 10^{-2}(k_s t)^{1/2} \text{ lbs/ft}^2, \text{ for } t \text{ in seconds}. \tag{72}$$

Differentiation of eq. (72) gives the rate of weight gain due to the parabolic oxidation and/or nitridation accretion, as

$$\frac{d}{dt}(\Delta m_s) = \frac{dW_1}{dt}\bigg|_{ch} = 1.7 \times 10^{-2}(k_s/t)^{1/2}. \tag{73}$$

This expression is to be multiplied by the surface area and then substituted into the re-entry equations for the accretion component of dW/dt, i.e., equations (2), (7), and (12a).
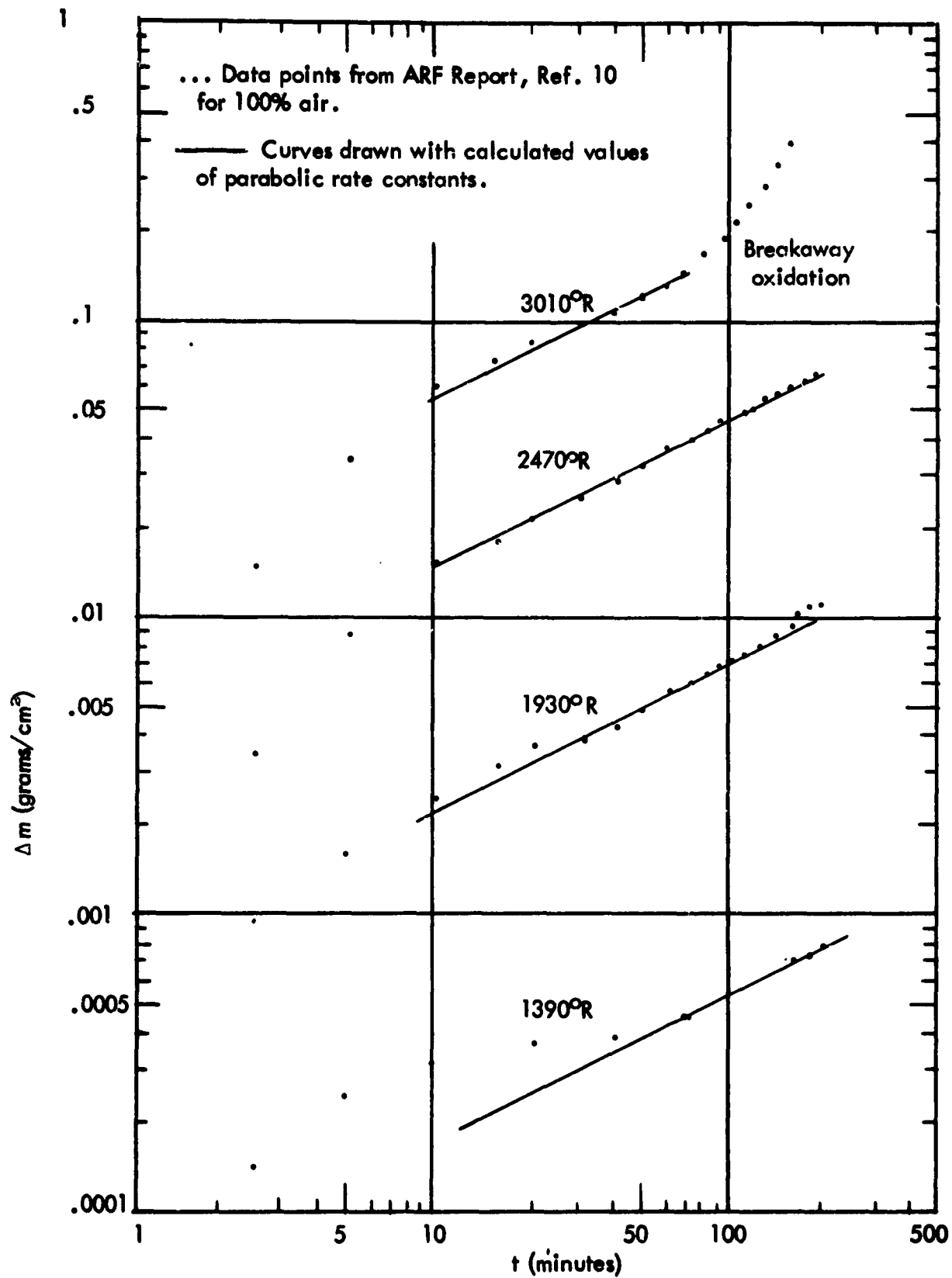
Figure 7. Effect of temperature on the oxidation of zirconium-uranium hydride in 100% air.
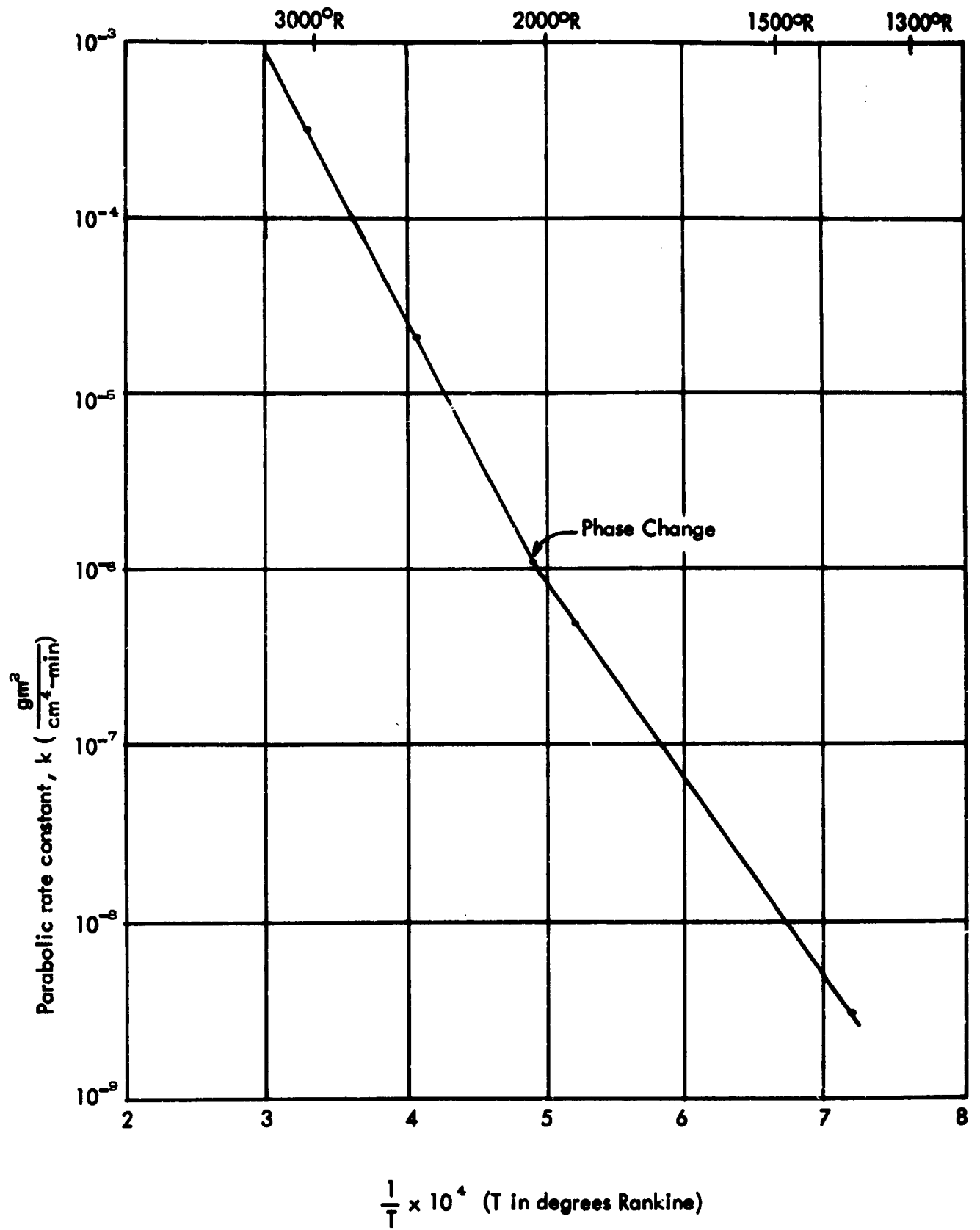
Figure 8. Variation with temperature of reaction rate constant for oxidation of zirconium-
uranium hydride.

2. Evaluation of H_{ch}

For the reaction $Zr + 2O \longrightarrow ZrO_2$, the heat energy released is, according to Wicks and Block,[30] for T in degrees Kelvin, given by the following equations.

$$H_{ZrO_2} = 262,960 - 2.65T + 1.6 \times 10^{-4}T^2 - 2.09 \times 10^5 T^{-1} \text{ cal/mole of } ZrO^2$$

$$\text{for } 298^\circ K \leq T \leq 1,135^\circ K. \quad (74)$$

$$H_{ZrO_2} = 264,360 - 2.21T - 4 \times 10^{-4}T^2 - 2.96 \times 10^5 T^{-1}, \quad 1,135^\circ K \leq T \leq 1,478^\circ K. \quad (75)$$

$$H_{ZrO_2} = 262,400 - 3.37T + 5.0 \times 10^{-4}T^2 + 4.0 \times 10^4 T^{-1}, \quad 1,478^\circ K \leq T \leq 2,100^\circ K. \quad (76)$$

Wicks and Block also give the following relations for the heat released in the reaction $Zr + N \longrightarrow ZrN$.
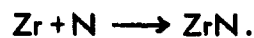
$$H_{ZrN} = 87,870 - 0.94T - 2.5 \times 10^{-5}T^2 - 8.5 \times 10^4 T^{-1}, \quad 298^\circ K \leq T < 1,135^\circ K. \quad (77)$$

$$H_{ZrN} = 89,110 - 0.40T - 5.8 \times 10^{-4}T^2 - 1.72 \times 10^5 T^{-1}, \quad 1,135^\circ K \leq T \leq 1700^\circ K. \quad (78)$$

These values are in calories per mole, with T in $^\circ K$. The equivalent increase in weight due to the formation of a mole of ZrO_2 over that due to the formation of a mole of ZrN is $32/14 = 2.28$. When this last expression is multiplied by 2.28, the result is

$$2.28 H_{ZrN} = 203,000 - 0.915T - 1.33 \times 10^{-3}T^2 - 3.93 \times 10^5 T^{-1}.$$

These relations show that the heat energy input to the fuel rod per unit weight gain is not markedly different for the formation of ZrO_2 and ZrN. Further, the heat of formation of UO_2 is almost identical with that of ZrO_2. Therefore, it makes little difference which reaction is responsible for the weight gain insofar as H_{ch} is concerned. The ratio of the heat energies released per unit weight gain by the fuel element, that is, $(H_{ZrO_2}/2.28 H_{ZrN})$ for T = 300, 600, 900, 1200, 1500, and 1700°K, are, respectively, 1.32, 1.32, 1.32, 1.31,

44

1.31, and 1.31. Further, chemical analysis on samples of fuel element material (see Appendices I and II show that, at most, a few percent of the weight gain can be attributed to ZrN. Thus, the use of only the heats of reaction of ZrO_2 will result in errors of less than a percent or so. That is, if all of the reactions are considered to lead to the formation of ZrO_2, the error would be less than about 1%.

3. Determination of $\dot{H}_{ch}$

The value of $\dot{H}_{ch}$ is determined by eq. (12a), together with the values of H_{ch}, M_r, and M_{ch}. That is,

$$\dot{H}_{ch} = \frac{H_{ch}}{g(M_r - M_{ch})} \frac{dW_1}{dt}\bigg|_{ch} . \tag{79}$$

The value of M_r is simply the molecular mass in slugs of Zr, i.e., $91.22/454 \times 32.2 = 6 \times 10^{-3}$ slugs/mole, while the appropriate value of M_{ch} is M_{ZrO_2}, or $123.33/454 \times 32.2 = 8.45 \times 10^{-3}$ slugs/mole. The value of $\frac{dW_1}{dt}\bigg|_{ch}$ is given by eq. (73), and H_{ch} is given by eqs. (74), (75), and (76).

F. DETERMINATION OF $G(T_w)$

This parameter, which constitutes the rate of loss of hydrogen from the fuel element, represents one of the weakest theoretical links in the re-entry model in that the data available were insufficient to evaluate the parameters in $G(T_w)$ with any high degree of confidence. An insight into the magnitude of the effects due to transpiration cooling can be gained as follows. If all of the hydrogen is presumed to transpire during the peak heating portion of the re-entry trajectory, then the calculated net heat input to the rod would be less than that in the actual re-entry case, whereas, if one presumes that no hydrogen is released during the re-entry,

45

the calculated net heat input to the rod would be greater than that in an actual re-entry case. An elementary calculation, based on eq. (9) and the dynamic heating curves for a fuel element presented in the North American Aviation Corporation's report (ref. 33) shows that these two bounds differ markedly. That is, if the entire hydrogen content of the fuel element were to transpire during the peak heating portion of the re-entry trajectory, the maximum temperature of the fuel element would be about $3000^\circ R$, whereas, without hydrogen transpiration, the fuel element is expected to reach its melting temperature (calculations based on re-entry from 300,000 feet, $1000^\circ R$ initial fuel rod temperature, re-entry angle of -0.25 degrees, and a re-entry velocity of 24,200 ft/sec). Now that the possible magnitude of this effect has been put in proper perspective, the mathematical representation for the rate of hydrogen loss will be presented.

The process of hydrogen loss is considered to be the following one: The hydrogen is released from the fuel material in accordance with a linear rate constant λ which depends upon the temperature of the material. The amount of hydrogen released per unit area of fuel element surface in a time t is

$$M_{Hr} = M_{Ho}\left[1 - e^{-\lambda t}\right] \qquad (80)$$

where M_{Ho} is the initial hydrogen mass per unit area of fuel element material. (See Appendix II for a complete formulation of this problem.) The ARF data provides a means whereby λ can be evaluated. These data show that

$$\lambda = 1.01 \times 10^{-8} T - 1.92, \text{ for } T > 1900^\circ R, \text{ and } t \text{ in minutes.} \qquad (81)$$

The value of λ is taken as zero for $T < 1900^\circ R$. In the meantime, an oxide (and/or nitride) layer has been building up on the surface of the rod, and the hydrogen must diffuse through this

46

layer in order to escape. This gives rise to a build-up of released hydrogen concentration, $M_{Hr} - \Delta m_H(t)$, within the boundaries of the oxide layer. Here, $\Delta m_H(t)$ is the mass of the hydrogen (per unit area of surface) that has escaped through the surface. Since the concentration of hydrogen outside of the oxide layer can be considered as being essentially zero, the rate of hydrogen diffusion through the oxide layer is expected to be (for a diffusion process) proportional to $\left[M_{Hr} - \Delta m_H(t) \right] / \Delta m_s$. Substituting the right-hand side of eq. (80) for M_{Hr} into this expression gives

$$\frac{dW_1}{dt} = \frac{d}{dt}\left[\Delta m_H(t) \right] = -a \left\{ \frac{\Delta m_H(t) - M_{Ho}\left[1 - e^{-\lambda t} \right]}{(k_s t)^{1/2}} \right\} = G(T_w)\frac{grams}{cm^2-min} \qquad (82a)$$

where a is the constant of proportionality, or what might be termed the diffusion constant. Here k_s is taken from eq. (70), using the values of A_s and Q_s given in eq. (71). To convert eq. (82a) into units suitable for use in eq. (12b), it must be multiplied by 1.06×10^{-3} to convert to slugs/ft^2-sec and by the area of the fuel element to obtain $G(T_w)$ in slugs/sec, i.e.

$$G(T_w) = 1.06 \times 10^{-3} \, S\frac{d}{dt}\left[\Delta m_H(t) \right] . \qquad (82b)$$

Equation (82a) must be integrated to obtain $\Delta m_H(t)$. This integration gives (see Appendix II)

$$\Delta m_H(t) = \frac{a M_{Ho}}{k_s^{1/2}} \, \exp(2a\sqrt{t/k_s}) \left\{ \frac{k_s^{1/2}}{a}\left[1 - \exp(2a\sqrt{t/k_s}) \right] \right.$$

$$- \frac{2a}{\lambda k_s^{1/2}}\left[1 + \exp(-2a^2/\lambda k_s) \right]$$

$$+ 2(t^{1/2} + a/\lambda k_s^{1/2})\left[1 + \exp(-2a^2/\lambda k_s) \right]\exp(-\lambda t + 2a\sqrt{t/k_s})$$

$$\left. + 2\sqrt{2\pi} \, \exp(-a^2/\lambda k_s)\left[erf(\sqrt{\lambda t} + a/\sqrt{\lambda k_s}) - erf(a/\sqrt{\lambda k_s}) \right] \right\} . \qquad (83)$$

47

The value of a must be determined from experimental data. Using sample fuel element specimens (provided by ARF and SRI) that had been exposed to oxidation and simulated re-entry tests, values of $\Delta m_H(t)$ were determined by chemical analysis (See Appendix I). With the reported values of M_{Ho} and these measured values, eq. (83) was used to determine a. Because t was very large for the oxidation data that were available, Δm_H was nearly equal to M_{Ho}. Thus, the scatter in the data on M_{Ho} casts considerable doubt on the values of a so determined. The value of a, based upon this limited data, was estimated to be

$$a = 0.10 \, e^{-1.84 \times 10^4/T} \, grams/cm^2 - min. \tag{84}$$

Although this expression may not be very accurate in general, the effects involved are so important that it should be used until more accurate data are available. It would not be difficult to determine an accurate value of a by resorting to experimental methods, e.g., weight gain measurements in an oxidizing atmosphere.

The value of M_{Ho} is determined by dividing the fuel element area by the mass of the total hydrogen contained in the fuel element.

G. DETERMINATION OF H_f, H_v, T_{wf}, F_c, F_v, H_{deG}, AND $H_{c, deG}$

1. Heat of Fusion, H_f, and Heat of Hydration, H_{deG}

These quantities can be taken directly from the report by Elliott.[32] According to this report, the fuel element material melts at 3825°R, and the heat of fusion is

$$H_f = 90 \, Btu/lb = 2.9 \times 10^3 \, Btu/slug. \tag{85}$$

Also, the report gives the hydrogen release energy as

$$H_{deG} = -610 \, Btu/lb \text{ of } Zr \cdot U \cdot H = 1.13 \times 10^6 \, Btu/slug. \tag{86}$$

2. Heat of Vaporization, H_v and T_{wf}

Although there is some question as to where the data originated, the heat of vaporization, according to a NAAI report,[33] is

$$H_v = 180 \text{ Btu/lb} = 5.8 \times 10^3 \text{ Btu/slug}. \tag{87}$$

This report implies that the vaporization takes place at a temperature of $4460°R$, hence, the appropriate value of T_{wf} would be

$$T_{wf} = 4460°F. \tag{88}$$

A calculation would then have to be made to see if, in accordance with eq. (11), the fuel element temperature would remain constant. If it would, then the fraction of the material that is vaporized is

$$F_v = 1. \tag{89}$$

If, under these conditions, the fuel element temperature drops, as determined by eq. (11), then the vapor pressure of the melted material will have to be known unless it can be shown that the fuel element breaks up at a temperature that is less than T_{wf}. All presently known data indicate that the fuel element material will remain intact until the metal at the oxide layer-metal interface melts. For this reason, the thermal expansion of the fuel element material has not been considered in the foregoing treatment.

It can readily be shown from kinetic theory that the particle flux, leaving a surface whose vapor pressure is P_v in millimeters of Hg, is given by the relation

$$\text{Flux} = .119 \, P_v \left[\frac{5 \, M_{de}G}{9 T_w} \right]^{1/2} \text{ lbs/ft}^2\text{-sec} \tag{90a}$$

where $M_{de}G$ is the gram molecular weight of the evaporating material, in the case of zirconium,

91.22. Equation (90) can be multiplied by S and divided by g and then substituted into the left-hand side of eq. (11) or (13), as appropriate, to keep track of the transpiration cooling effect on dT_w/dt and hence on T_w. That is,

$$-\frac{1}{g}\frac{dW}{dt} = \frac{0.119S}{g}\left[\frac{5\,M_{deG}}{9\,T_w}\right]^{1/2}\text{ slugs/sec.}\tag{90b}$$

Equation (90) can also be employed to show that there will be no dearth of oxygen present in the boundary layer for oxidation purposes during re-entry simply by setting $M_{deG} = 32$, the molecular mass of oxygen, and using the local boundary layer pressure for P_v. Such a calculation shows that the flux available (at altitudes below 300,000 ft) is certainly much greater than can be used in the oxidizing process.

3. Heat of Combustion or Recombination, $H_{c, deG}$, and F_c

There is a possibility that the evolved hydrogen atoms will recombine and then burn with the oxygen in the boundary layer. If the hydrogen recombines, the energy release is approximately 3×10^6 Btu/slug (≈ 104 k cal/mole of H_2). This number is to be used as $H_{c, deG}$ for the hydrogen recombination. If the hydrogen, after recombination, reacts with the oxygen in the boundary layer, the net energy release will be approximately 3.5×10^6 Btu/slug of of H_2 (120 k cal/mole of H_2). Since the activation energy for the formation of H_2 from H atoms is zero, it follows that the net heat energy release would be the sum of these last two energies (i.e., approx. 6.5×10^6 Btu/slug of hydrogen used) if the reaction went straight through to form water without the hydrogen recombination step.

In view of the facts that the burning rate of hydrogen in oxygen is less than Mach 1, the boundary layer is very thin, and the activation energy for H_2O production is 104 k cal/ mole of H_2O, it is reasonable to assume that the hydrogen will diffuse well into the boundary

50

layer before any appreciable portion of it goes into the production of water. Thus, the addition of the combustion energy of hydrogen to the total energy content of the boundary layer is expected to make only a small contribution to this total energy content. Consequently, it seems reasonable to assume that F_c can be considered to be very small for the combustion of H_2 and that the H_2 combustion will make a negligible contribution to the total heat flux into the fuel rod during re-entry.

The case for neglecting the effects due to the heat of recombination of hydrogen during the re-entry of the fuel element is not nearly so clear cut as is the case for neglecting the combustion of the hydrogen. None of the data available to the authors provides information from which F_c for hydrogen recombination can be estimated. In view of the fact that the recombination energy of the total quantity of hydrogen contained in the fuel element is about 5,500 Btu's (based on the formula $ZrH_{1.85} - U_{.0432}$), it is almost as large as the total aerodynamic heat energy available to the fuel rod during re-entry. The latter quantity is only some 6,000 Btu's.

There is the possibility that some of the evolved hydrogen would combine at grain boundaries or in cracks within the fuel element, and some of it might combine beneath the oxide layer. Again, some of it might be evolved before the stainless steel cladding on the fuel element has burned off and, thus, recombine between the fuel material and the cladding. However, this latter possibility seems remote because the stainless steel cladding is insulated from the fuel material by a ceramic which is a poor heat conductor.

It is clear from the foregoing discussion that additional research is required before an understanding of what happens to the hydrogen in the fuel element can be realized.

51

IV. SUMMARY STATEMENT

Although the effect of the fuel element cladding has not been considered here, it is obvious that the same treatment is applicable. The treatment of this part of the problem that was presented by NAAI[33] should not prove grossly in error when used with the foregoing re-entry heating equations.

If the effects due to the recombination and combustion of the hydrogen content of the fuel element can be neglected (it seems likely that the effects due to combustion, at least, can), then bounds of the upper temperature that the fuel element will attain during re-entry can be calculated with a high degree of confidence for the following three cases: 1) no transpiration cooling; 2) all hydrogen transpires at the phase change temperature (approx. 2040°R); 3) all hydrogen transpires during the peak heating portion of the re-entry trajectory.

In the case where no hydrogen transpires, a hand calculation, using the NAAI[33] data, indicates that the entire fuel element will be melted by re-entry heating. If the hydrogen is all evolved at a fuel rod temperature of 2040°R (phase change temperature), the estimated peak temperature of the fuel element is, based on hand calculations, approximately 4000°R. If it all evolves during the peak heating portion of the re-entry trajectory (starting at about 2800°R), hand calculations indicate that the peak temperature of the rod will be approximately 3000°R. The incident heat flux used in these calculations was taken from curves presented in ref. 33 for re-entry from an altitude of 300,000 feet at 24,200 ft/sec and an initial trajectory angle of -0.25 degrees. The continuous transpiration theory derived in the foregoing analysis does not lend itself readily to a hand calculation and was not attempted by the authors.

Exclusive of the behavior of evolved hydrogen, the values of the various parameters in the re-entry equations, as given above, are quite good. Although one hesitates to place

52

accuracy limits on the entire mathematical model, it seems unlikely that the cumulative error resulting from errors in the values of the parameters given above would exceed 10% for temperatures up to the melting point of the fuel material.

The hydrogen transpiration data presented above is quite susceptible to error because of the poor quality of the initial data that was available to GTC. This is not meant to reflect poor quality work on the part of other researchers who produced this initial data, because the experiments and tasks they performed on the sample materials supplied to GTC for analysis were not designed to produce the type of data that GTC's analysis showed to be required.

At the present time, there is no data available, to the authors' knowledge, from which information on the magnitudes of possible effects due to hydrogen recombination can be deduced. Also, the vapor pressure data on the zirconium-uranium alloy could not be uncovered. Thus, the value of the parameters F_c and F_v are undetermined at this time.

It should be borne in mind that the chemical reactions deduced in this study will not necessarily obey the same laws once the metal becomes molten under the oxide layer. At this point, the metal cations may diffuse to the surface while the oxide is diffusing to the molten material. As has been shown by Littman, the oxide forms a solution with the metal when the metal is in a molten state.[44] If there is no cation diffusion through the oxide, then the continued oxidation of the molten metal would surely disrupt the oxide surface layer because the density ratio[27] of Zr to ZrO_2 is approximately 2. If the oxide layer is thus broken off, the portion of the rod material that is in a molten state will blow off in drop or droplet form, in which case the theory of Opik[45] determines the maximum size of the particles. The portion of the rod that is in a molten state at any time can be calculated from the system of re-entry equations derived above and eq. (14). Whether or not further droplets will be released after this initial release, should such an initial release occur, will depend on the vapor pressure,

53

the surface tension, the viscosity, etc. of the molten material. It seems likely that the zirconium does diffuse to the surface to relieve the internal pressure built up by the absorbed oxide, because Littman found that when cubes of the fuel element material have an oxide layer on their surface, they retain their shape when inductively heated even though the metal inside is in a molten state. If this is the case, then the fuel element will re-enter intact unless breakaway oxidation or angular acceleration forces due to tumbling and spinning cause the oxide layer to break off. Although this report shows the point of breakaway oxidation for anion diffusion, this value is not expected to be valid when both anion and cation diffusion take place simultaneously. The accelerating forces can be calculated from the foregoing equations of angular motion. Should it turn out that the material below the oxide layer becomes molten, that the oxide layer is thin, and that the angular acceleration forces are large, the oxide layer could be broken to expose the molten surface to viscous drag shearing forces which will produce molten drops. All this will remain speculative until the actual calculations are performed.

V. REMAINING RESEARCH TO BE ACCOMPLISHED

At this point in the entire SNAP fuel element re-entry program, it is quite clear what remains to be done to ascertain whether or not the fuel elements will burn up during re-entry. This could be accomplished in steps as follows:

First, the research necessary to determine F_c and F_v, together with a better value of a would be carried out. Then, using the foregoing analytical, mathematical model, a machine calculation would be performed to determine if any substantial portion of the fuel element will reach the melting point. If it will not, then the fuel element will not burn up during re-entry. It is apparent that the upper bound heat input case (transpiration cooling plus hydrogen recombination) should be employed in the first calculation. Thus, if this calculation were to show that the fuel element would burn up, there is strong evidence that it could be made to burn up during re-entry.

The final step would be to try to find out how much of the fuel element would be ablated away. This would require a detailed knowledge of the amount of material that blows off in droplet form and from which part of the fuel rod this material is released so that the aerodynamic parameter changes could be accounted for. This assumes that $F_v \neq 1$. Should research show that $F_v = 1$, then the foregoing calculation would be conclusive. In this latter case, a good approximation to the degree of burn-up could be obtained by assuming that the material evaporates uniformly from the surface of the rod and by using the same set of equations given above with diminishing diameter. The result of this calculation would be the minimum size of the fuel rod that could survive the re-entry. If this is zero, then there is little to worry about from a safety point of view. If it is not zero, then the degree of hazard associated with the remaining material could be specified by safety personnel.

55

APPENDIX I

CHEMICAL ANALYSIS

This appendix contains a general discussion of the behavior of zirconium and zirconium-uranium alloys in various gases. The chemical analyses and results obtained by GTC are also presented. A description of the samples of fuel element materials which GTC received during the contract is presented in tabular form.

A. REVIEW OF PREVIOUS STUDIES ON OXIDATION OF ZIRCONIUM AND THE EFFECTS OF O_2, N_2, H_2 ON ZIRCONIUM

Since preliminary X-ray data indicated that, on the oxidation specimens provided to GTC by the Armour Research Foundation, only ZrO_2 was present in the outer layer of the specimen, the decision was made to survey previous investigations on the kinetics of the oxidation of zirconium.

The reaction of zirconium with oxygen at various temperatures has been studied by several investigators. A comparison of the results shows discrepancies concerning the order of the rate law (cubic, parabolic, or linear) which best fits the oxidation curves. Hayes and Roberson[34] undertook a qualitative study of this subject by heating panels of Zr in various gases. They found that above 800°C, oxygen diffuses into the grain structure of the metal when heated in an oxygen atmosphere at 1 atm pressure. It appears probable that the oxygen penetration into the grain boundaries takes place at 862°C, when the close-packed hexagonal alpha phase transforms to the body centered cubic beta form. The two percent volume change and phase transformation certainly provides the opportunity for intergrunular oxygen diffusion. They also found that heating to 900°C in moist air (percentage of water vapor not given) produced a 15 to 18 percent volume increase of the specimen, which they attributed to the oxide

56

formation. However, heating in dry air or oxygen showed no perceptible change in size. Also, heating to temperatures above 1000°C in nitrogen produced a nitride film, and nitrogen diffused into the metal, but the nitride film formed was permeable to oxygen at 1000°C.

Hayes and Roberson came to the conclusion, that when heated in air, Zr undergoes simultaneous attack by both oxygen and nitrogen. The nitride was found to be unstable in the presence of oxygen, and decomposed to a voluminous oxide.

Gulbransen and Andrew[35] studied the reaction on zirconium foil specimens between 200°C and 425°C. They reported that a modified parabolic rate law fits the data. The temperature dependence of the oxidation rate as a function of film thickness showed a constant relationship. This fact suggests that one mechanism is controlling the rate over a wide thickness range.

In another study, Gulbransen and Andrew[36] found that between 400° and 800°C, the method of surface preparation influenced the reaction kinetics. Mechanically polished foils obeyed the cubic rate law and reacted faster than chemically polished foils, which obeyed the parabolic rate law.

A later study by Charles, Barnartt, and Gulbransen,[37] on the prolonged oxidation of zirconium foils up to times of 500 hours and temperatures of 350° to 450°C, confirmed the cubic rate law for mechanically polished specimens. However, there is sufficient reason to suspect that the size and shape of the zirconium samples may influence the reaction kinetics. Belle and Mallett[38] studied the oxidation reaction on machined cylindrical specimens 4 cm long by 0.7 cm, and 5 cm long by 1.4 cm. They found that a cubic rate law fit the data taken from 575°C to 950°C at one atmosphere of pure oxygen, while on foil specimens in approximately the same temperature range, several other investigators observed a parabolic rate law fit.

There is also evidence that the particular rate law which the reaction follows depends on the temperature range. In a recent study by Kofstad,[89] zirconium was oxidized under conditions of linearly increasing temperature. It was shown that between 650° and 950°C, the cubic rate law was obeyed, and between 950° and 1100°C, the parabolic rate law fit the data. This is in close agreement with the analysis of the ARF data presented in the text of this report.

Some investigation has also been done on the effect of pressure on the oxidation of zirconium. Gulbransen and Andrew, among others, came to the conclusion that pressure has little or no effect on the reaction of zirconium with oxygen.

The reaction of zirconium with nitrogen has been shown to proceed at a much slower rate than has been found for the reaction with oxygen. Several studies have been made (see references 34 and 35), and most investigators agree that the parabolic rate law is consistent with the data at the higher temperatures. The product of the reaction in nitrogen at all temperatures has been identified as ZrN. Gulbransen and Andrew[34] noticed that small amounts of oxygen in the nitrogen noticeably accelerate the rate of the reaction. Draunieks[40] found that at temperatures from 862° to 1043°C, the nitrogen diffuses into the metal as well as precipitates a nitride film on the surface.

Some work has also been done on the reaction of zirconium and zirconium alloys with air. In general, the reaction rate is more rapid in air than in either oxygen or nitrogen alone. In this case, the solubilities of oxygen and nitrogen in the metal will form solid solutions of the gases in the metal phase as well as phase formation of ZrO_2 and ZrN. According to Gulbransen, for the zirconium oxygen reaction, the overall rate of oxygen absorption still remains parabolic, if the rates of both the penetration of the gas into the metal and the growth

of the oxide layer are diffusion controlled, and the diffusion constants remain constant. The same type of reasoning can be applied to the nitrogen reactions.

Gulbransen and Andrew[35] also studied the rate of hydrogen diffusion into zirconium at 300°C. They found that at constant temperature the reaction rate could be expressed as

$$\frac{dW}{dt} = A \, p^{\frac{1}{2}} \, ,$$

where p is the pressure of the hydrogen atmosphere and A is a constant. According to theory, this rate-pressure relation is an indication of activated diffusion with dissociation. Therefore, the correlation shows that the diffusion of hydrogen into zirconium is mainly by atoms of hydrogen. Additional information on the dissociation rates of hydrogen can be derived from the data presented by Atkins.[41] These data show that the equilibrium concentration of hydrogen in $Zr:H:U$ is very nearly independent of the external hydrogen pressure, varying from the one-eighth to the one-fourteenth power of the pressure.

The crystal structure of ZrO_2 has been studied by several investigators. Zirconium dioxide has been shown to exist in three crystalline modifications — monoclinic, cubic, and tetragonal.[35] The monoclinic form which has been found by most investigators is a close packed arrangement with oxygen spacings of 2.6 to 2.7 Å. A consideration of the ionic radii of Zr^{+4}, 0.90 Å, and O^{-2}, 1.36 Å, shows that the oxygen ions could occupy interstitial positions in the ZrO_2 lattice. Thus, the oxidation rate is expected to be controlled by the rate of diffusion through the oxide layer.

B. RESULTS OF CHEMICAL AND PHYSICAL ANALYSES

The problem was approached by using various techniques of chemical and physical analysis to obtain data from certain selected ablation and oxidation samples, for the purpose

of formalizing and substantiating a burn-up model of the zirconium-uranium-hydride fuel element.

The samples were provided to GTC by Air Force contractors, namely, Vidya Division of the Itek Corporation, Astropower, Inc., Stanford Research Institute, Battelle Memorial Institute, and the Armour Research Foundation. As the samples were received by GTC, they were tabulated along with the simulated conditions under which they were tested (see Table 5). All samples which had been prepared for metallographic study were examined under a microscope for the presence of cracks, voids, oxidation layers, disrupted grain boundaries and grain structure.

The samples to be subjected to X-ray and chemical analysis were chosen on the basis of the test conditions to which they were exposed. A selection was made of twenty samples to be chemically analyzed, and five samples were used for X-ray analysis.

For the determination of compounds produced by the effects of ablation and oxidizing conditions, a determination of crystal structures was made by X-ray diffraction. Although this method is limited to qualitative results, the identity of the major compounds which are involved in the process was established.

The X-ray data were taken on a Siemens X-ray diffraction unit, using a 30 kilovolt source with 20 ma K-α Cu radiation. The patterns were scanned at 0.5° per minute from 15° to 110° with a 2% statistical error. The peaks were checked against the 1962 NBS card data file for the following compounds:

1. Both α and β phase zirconium dioxide (ZrO_2)
2   Uranium metal (U)
3. Uranium nitride (UN)
4. β Uranium metal (βU)
5. Diuranium pentaoxide (U_2O_5)
6. Three phases of triuranium octaoxide (U_3O_8)

60

7. α and β uranium dioxide (UO_2)
8. Uranium trioxide (UO_3)
9. Uranium-zirconium (U-Zn)
10. Zirconium nitride (ZrN)

The results of this analysis are given in Table 3.

TABLE 3

X-RAY DIFFRACTION RESULTS

GTC Nr.	Material	Test Temp. (°C)	Air-Argon Atmosphere (% Air)	Sample Condition	Compounds Identified
26	Zr-U-H	1100	50	Powdered outer layer	ZrO_2, possibly uranium metal
20	Zr-U-H	800	50	Surface film	Results cannot be identified, possibly because of interference due to substrate layer
25	Zr-U	1100	50	Surface film	Results cannot be positively identified, but ZrO_2 indicated
28	Zr-U-H	1100	100	Surface film	ZrO_2 only
32	Zr-U-H	1400	50	Powdered outer layer	Very strongly ZrO_2 (24 peaks matched)

The chemical analysis of the samples was made by a vacuum fusion technique. This type of analysis gives the weight percentages of oxygen, nitrogen, and hydrogen remaining in the samples after testing under simulated ablation conditions. Because the samples are all inorganic substances with high melting points and a quantitative measure of the combined and absorbed gases is necessary to supply data for the reaction constants and hydrogen evolution rate, the high temperature vacuum technique is about the only method by which the small amounts of samples can be analyzed.

61

Where possible, certain samples were analyzed in two parts. One part consisted of the surface layer, composed mainly of ZrO_2 and the other part was the center core of the sample minus the surface layer. This technique provided information on the amount of oxygen and nitrogen which had diffused into the center section of the fuel element.

The results of the vacuum fusion analysis for the twenty samples appear in Table 4.

Since S.R.I. ran samples under constantly changing conditions comparable to re-entry trajectories, only generalizations can be made about the results. It appears that up to 3000^oR, a significant amount of hydrogen is retained by the sample. It also is apparent that the build-up of an oxidation layer on the surface presents a definite barrier to the evolution of hydrogen, even up to 3500^oR. Furthermore, it is apparent from I.I.T.R.I. samples that the hydrogen is retained in the samples up to 1100^oC regardless of the amount of oxide formation on the surface of the sample. In most cases, at temperatures of 1100^oC and upward, a large amount of oxygen is present in the surface layer, and some of the oxygen has managed to diffuse into the center core of the sample. Judging from the increases in the nitrogen content of some of the samples nitrogen combination or absorption plays some role in the chemical kinetics of the ablation process, although its role is not nearly as significant as that of oxidation reactions. Unfortunately, no conclusions can be derived concerning the effects or probability of a hydrogen-oxygen reaction from the data presented. In certain cases, the loss of hydrogen may be responsible for a decrease in oxidation, while in other cases it may promote oxidation.

An interpretation of the analytical results in terms of specific reactions is difficult because the effects are of an integrated nature and therefore difficult to separate experimentally. However, the data were most helpful in determining reaction rate constants, in establishing the order of the oxidation rate law, and in determining the diffusion coefficient for the hydrogen loss.

TABLE 4

VACUUM FUSION ANALYSIS OF SAMPLES

GTC No.	Material	Test Temp.	Atmosphere	Sample Condition	Gas Analysis (Wt.%)		
					Oxygen	Nitrogen	Hydrogen
Blank (A.I. Material)							
0 (blank)	Zr-U-H	None	None	Chunk	.064	.019	1.64
Stanford Research Samples							
51-H	Zr-U-H	3500°R	Air	Pyramid	.139	.028	.073
53-H	Zr-U-H	3840°R	Air	Pyramid	.420	.169	.020
56-H	Zr-U	3590°R	Air	Half-Pyramid	2.800	.800	.003
56-H	Zr-U-H	3550°R	Air	Half-Pyramid	3.980	.070	.148
40-H	Zr-U-H	2940°R	Air	Pyramid	.065	.012	.476
I.I.T.R.I. (Formerly Armour Research) Samples							
12	Zr-U-H	500°C	Ar - 10% Air	1/2 Disk	.289	.017	1.078
16	Zr-U-H	500°C	100% Air	1/2 Disk	.386	.109	1.000
18	Zr-U-H	800°C	Ar - 10% Air	1/2 Disk	1.022	.067	.930
21	Zr-U	800°C	100% Air	Fragments	.146	.002	.005
22	Zr-U-H	800°C	100% Air	Fragments	.231	.002	1.130
24(a)	Zr-U-H	1100°C	Ar - 10% Air	1/2 Center core	1.050	.082	.008
24(b)	Zr-U-H	1100°C	Ar - 10% Air	Surface layer	4.028	.508	.014
27(a)	Zr-U	1100°C	100% Air	Fragments of center core	.048	.009	.002
27(b)	Zr-U	1100°C	100% Air	Surface layer	.638	.613	.014
28	Zr-U-H	1100°C	100% Air	Fragments	.613	.025	.995
30(a)	Zr-U-H	1400°C	Ar - 10% Air	Core	3.160	.127	.027
30(b)	Zr-U-H	1400°C	Ar - 10% Air	Surface layer	11.992	2.202	.015
33(a)	Zr-U	1400°C	100% Air	Core fragments	1.350	.025	.008
33(b)	Zr-U	1400°C	100% Air	Surface layer	8.930	.006	.010
Vidya Sample							
5	Zr-U-H	Unknown	Air	Surface layer from exposed surface of cylinder	3.695	.354	.035

TABLE 5
TABULATION OF SAMPLES
A. Vidya Samples

All models were one inch diameter cylinders of hydrided fuel rod material. Atmosphere; dry air.

Sample No.		Avg. cold wall heat rate[a] (BTU/ft^2-sec)	Stagnation enthalpy H_{st} (BTU/lb)	Stagnation pressure at model surface P_{st} (psia)	Model weight change (grams)	Run duration (seconds)
G.T.C.	Vidya					
1	538	104	6380	14.7	0.000	60
1a	544[b]	845	3770	16.2	-64.49	59.5
2	539	605	2280	19.0	-.350	60
3	550	868	3180	19.9	-59.40	60
4	551	163	4930	14.7	+.016	121
5	552	582	3980	16.0	+.262	62.3
6	553	93	7080	14.7	+.020	121.3
7	554	574	3810	16.0	-49.187	92
8	555	453	4680	15.5	-.062	61
9	556	876	3230	19.0	+.341	70.4
10	557	435	4630	15.5	+.228	120.2

Notes: a. Heat rate averaged over the surface of a flat face or hemispherical surface of a cooled copper calorimeter of the same size and geometry as the test model.

b. Rerun of run 538 with nitrogen as test fluid.

TABLE 5 (Continued)

B. Illinois Institute of Technology Research Institute Samples

In each case, the time of run was 3 hours, at 1 atmosphere pressure.

G.T.C. Sample No.	Composition	Air-Argon Atmosphere (% Air)	Heat flux or temp. (°C)	Comments
11	Zr-U	10	500	Grey outside, thin layer
12	ZrH-U	10	500	1 mil thick outside layer
13	Zr-U	50	500	Grey outside layer
14	ZrH-U	50	500	Small cracks around edges
15	Zr-U	100	500	Needle-like grain structure but no oxide formation
16	ZrH-U	100	500	Shows distorted grain boundaries
17	Zr-U	10	800	Grey-white outside layer
18	ZrH-U	10	800	Definite oxide layer, distorted grain boundary near edges
19	Zr-U	50	800	Grey-white outside layer
20	ZrH-U	50	800	1-1/2 mil thick outside layer, disruption of grain boundaries
21	Zr-U	100	800	Grey-white outside layer
22	ZrH-U	100	800	Random grain structure near edges showing surface reaction
23	Zr-U	10	1100	Oxide layer 1/32 inch deep
24	ZrH-U	10	1100	Material flakes off surface
25	Zr-U	50	1100	Thin white oxide coat, grey beneath
26	ZrH-U	50	1100	Silver-grey oxide layer, gold flecked beneath

TABLE 5 (Continued)
B. Illinois Institute of Technology Research Institute Samples (Continued)

G.T.C. Sample No.	Composition	Air-Argon Atmosphere (% Air)	Heat flux or temp. (°C)	Comments
27	Zr-U	100	1100	White oxide layer on surface
28	ZrH-U	100	1100	Black pitted surface, cut and polished on one side
29	Zr-U	10	1400	Heavy oxide coating
30	ZrH-U	10	1400	Heavy oxide coating
31	Zr-U	50	1400	Heavy oxide coating (powdery)
32	ZrH-U	50	1400	Oxidized all the way through
33	Zr-U	100	1400	Oxidized all the way through
34	ZrH-U	100	1400	Cracked and spalling

Sample No. G.T.C.	S. R. I. Trajectory	Comp.	Heat Flux $\overline{\dot{q}_s}$ Avg. (BTU/ft^2-sec)	$\overline{\dot{q}_s}$ Actual	Temp. (°R)	System Pressure (in. of Hg.)	Time (sec.)	Comments
37	a-1	alloy	—	—	—	—	—	Not tested
38	1a-2	alloy	110	165	2350	0.1	100	Grey-white layer, cracked on one ridge.
			150	225	2560	0.2	100	
			265	395	2960	0.6	100	
			365	545	3140	2.0	50	
			215	120	2780	4.0	50	
			45	25	2240	2.6	50	
39	1a-4	hydride	110	165	2290	0.1	100	Grey coating, eroded on edges.
			150	225	2380	0.2	100	
			265	395	2830	0.6	100	
			365	545	3120	2.0	50	
			215	120	2890	4.0	50	
			45	25	2260	2.6	50	
40	1a-9	hydride	110	165	2260	0.1	100	Grey coating, eroded on edges.
			150	225	2350	0.2	100	
			265	395	2740	0.6	100	
			365	545	2940	2.0	50	
			215	120	2600	4.0	50	
			45	25	2220	2.6	50	
41	2a-6	alloy	365	545	3100	0.8	50	Grey-white coating, no erosion.
			360	540	2995	1.0	50	
			265	395	2650	1.9	50	
			100	150	2260	3.7	50	
			10	15	2095	1.6	50	
42	2a-9	hydride	365	545	2840	0.8	50	Grey coating, edges eroded.
			360	540	2350	1.0	50	
			265	395	2610	1.9	50	
			100	150	2260	3.7	50	
			10	15	2130	1.6	50	
43	3a-1	alloy	700	900	3480	4.5	20	Grey-white surface layer.
			340	510	3360	4.0	20	
			160	240	2470	4.4	20	
			40	60	2400	3.9	20	

Sample No. G.T.C.	S. R. I. Trajectory	Comp.	Heat Flux $\dot{q}_s$ Avg. (BTU/ft^2-sec)	$\dot{q}_s$ Actual	Temp. (°R)	System Pressure (in. of Hg.)	Time (sec.)	Comments
44	2b-1	alloy	245	360	2565	1.2	50	All white oxide
			450	675	3280	8.8	50	covered, ends and
			720	900	3515	36.8	50	edges split.
			400	600	3190	62.0	50	
45	3b-1	alloy	250	375	2470	10.4	35	Greyish-white, ends
			400	600	3300	44.0	35	and edges split open.
			240	360	2470	50.4	35	
46a	a-4	alloy	45	68	2200	*	300	Sectioned and potted,
			90	145	2350	.04	100	shows small amount of
			200	300	2710	.24	100	surface reaction.
			340	510	3090	1.40	100	
			140	210	2560	2.40	100	
46h	a-5	hydride	45	68	2190	*	300	Sectioned and potted,
			90	145	2280	.04	100	shows small amount of
			200	300	2440	.24	100	surface reaction.
			340	510	2930	1.40	100	
			140	210	2490	2.40	100	
47a	a-7	alloy	45	68	2330	*	300	Sectioned and potted,
			90	145	2090	.04	100	shows layer of surface
			200	300	3190	.24	100	reaction.
			340	510	3500	1.40	100	
			140	210	2800	2.40	100	
47h	a-9	hydride	45	68	2200	*	300	Sectioned and potted,
			90	145	2240	.04	100	shows layer of surface
			200	300	2510	.24	100	reaction.
			340	510	3010	1.40	100	
			140	210	2320	2.40	100	
48a	1a-3	alloy	110	165	2550	0.1	100	Sectioned and potted,
			150	225	2670	0.2	100	grain boundaries dis-
			205	395	2980	0.6	100	rupted near outer
			305	545	3120	2.0	50	surface.
			215	120	2750	4.0	50	
			45	25	2210	2.6	50	

*no data

Sample No. G.T.C.	S. R.I. Trajectory	Comp.	Heat Flux $\dot{q}_s$ Avg. (BTU/ft²-sec)	$\dot{q}_s$ Actual	Temp. (°R)	System Pressure (in. of Hg.)	Time (sec.)	Comments
48h	1a-1	hydride	110	165	2330	0.1	100	Sectioned and potted, grain boundaries disrupted near outer surface.
			150	225	2350	0.2	100	
			205	395	2820	0.6	100	
			305	545	3120	2.0	50	
			215	120	2890	4.0	50	
			45	25	2260	2.6	50	
49a	2a-7	alloy	365	545	2970	0.8	50	Sectioned and potted.
			360	540	3010	1.0	50	
			265	395	2670	1.9	50	
			100	150	2240	3.7	50	
			10	15	2095	1.6	50	
49h	2a-8	hydride	365	545	2830	0.8	50	Hydride is cracked along back edge. Sectioned and potted.
			360	540	2850	1.0	50	
			265	395	2615	1.9	50	
			100	150	2260	3.7	50	
			10	15	2132	1.6	50	
50a	3a-2	alloy	700	900	3500	4.5	20	Sectioned and potted.
			340	510	3320	4.0	20	
			160	240	2545	4.4	20	
			40	60	2420	3.9	20	
50h	3a-3	hydride	700	900	3140	4.5	20	Hydride cracked along back edge.
			340	510	3010	4.0	20	
			160	240	2400	4.4	20	
			40	60	2310	3.9	20	
51a	4a-5	alloy	480	720	3715	20.8	20	Sectioned and potted, alloy has surface reaction.
			140	210	2330	4.4	20	
			48	72	2110	2.4	20	
51h	4a-8	hydride	480	720	3500	20.8	20	Sectioned and potted, hydride is cracked.
			140	210	2185	4.4	20	
			48	72	2110	2.4	20	

Sample No. G.T.C.	S.R.I. Trajectory	Comp.	Heat Flux $\dot{q}_s$ Avg. (BTU/ft^2-sec)	$\dot{q}_s$ Actual	Temp. (°R)	System Pressure (in. of Hg)	Time (sec.)	Comments
52a	b-3	alloy	60	90	2470	0.2	400	Sectioned and potted, cracked.
			130	195	2600	0.4	200	
			320	480	3000	2.4	200	
			640	900	2650	18.4	100	
			320	480	3020	66.0	100	
52h	b-4	hydride	60	90	2470	0.2	400	Sectioned and potted, cracked.
			130	195	2550	0.4	200	
			320	480	2980	2.4	200	
			640	900	2650	18.4	100	
			320	480	2990	66.0	100	
53a	b-6	alloy	60	90	2510	0.2	400	Sectioned and potted, reaction layer around edges of specimen.
			130	195	2650	0.4	200	
			320	480	3155	2.4	200	
			640	900	3695	18.4	100	
			320	480	3155	66.0	100	
53h	b-8	hydride	60	90	2470	0.2	400	Sectioned and potted, reaction layer around edges of specimen.
			130	195	2615	0.4	200	
			320	480	3245	2.4	200	
			640	900	3840	18.4	100	
			320	480	3140	66.0	100	
54a	1b-3	alloy	65	100	2310	0.2	300	Sectioned and potted, definite layer around edges of sample.
			215	325	2490	1.2	100	
			415	625	3120	4.8	100	
			670	900	3640	30.0	100	
			240	360	2565	30.0	100	
54h	1b-4	hydride	65	100	2350	0.2	300	Sectioned and potted, definite layer around edges of sample.
			215	325	2435	1.2	100	
			415	625	3210	4.8	100	
			670	900	3720	30.0	100	
			240	360	2760	30.0	100	

	Sample No.			Heat Flux					
G.T.C.	S.R.I. Trajectory	Comp.	$\bar{q}_s$ Avg. (BTU/ft^2-sec)	$\bar{q}_s$ Actual	Temp. ($^\circ$R)	System Pressure (in. of Hg.)	Time (sec.)	Comments	
55a	1b-5	alloy	65	100	2110	0.2	300	Sectioned and potted.	
			215	325	2760	1.2	100		
			415	625	3660	4.8	100		
			670	900	3800	30.0	100		
			240	360	2740	30.0	100		
55h	1b-4	hydride	65	100	2145	0.2	300	Sectioned and potted.	
			215	325	2185	1.2	100		
			415	625	3280	4.8	100		
			670	900	3680	30.0	100		
			240	360	2650	30.0	100		
56a	2b-2	alloy	245	360	2510	1.2	50	Sectioned and potted.	
			450	675	3320	8.8	40		
			720	900	3590	36.8	50		
			400	600	3210	62.0	50		
56h	2b-4	hydride	245	360	2290	1.2	50	Sectioned and potted, hydride cracked, reaction layer around edges.	
			450	675	2940	8.8	40		
			720	900	3550	36.8	50		
			400	600	3110	62.0	50		
57a	3b-2	alloy	250	375	2580	10.4	35	Sectioned and potted, slight recovery zone on surface.	
			400	600	3190	44.0	35		
			240	360	2435	50.4	35		
57h	3b-4	hydride	250	375	2330	10.4	35	Sectioned and potted, slight recovery zone on surface.	
			400	600	3010	44.0	35		
			240	360	2330	50.4	35		

TABLE 5 (Continued)
D. Armour Research Foundation
Tested at 1 Atm. Pressure

Sample No. G.T.C.	Composition	Type of test performed	Atmosphere	Temp. (^oR)	Comments
58	ZrH–U	Loss of fuel rod integrity	Argon	3350	5 pieces showing zones of reaction.
59	ZrH–U	Linear thermal expansion	Hydrogen	2790	Long, rod–shaped piece.
60	Zr–U	Linear thermal expansion	Argon	2790	Long, rod–shaped piece.
61	ZrH–U	Thermal conductivity	Hydrogen	2710	1" rods, material flakes off.
62	Zr–U	Thermal conductivity	Argon	2750	1" rods, material flakes off.
63	ZrH–U	Emissivity	Air	2500	Round disks about 1.343"
64	ZrH–U	Emissivity	Hydrogen	2800	diameter, material flakes
65	ZrH–U	Emissivity	Argon	2800	off.
66	Zr–U	Specific heat	Argon	2770	Rod–shaped pieces, sur-
67	2 samples ZrH–U	Specific heat	Hydrogen	2700	face reaction.
68	Zr–U	Heat of fusion	Argon	3430	Encapsulated in graphite.
69	ZrH–U	Tensile test	Air	Room temp.	Broken at gauge mark.
70	ZrH–U	Tensile test	Air	Room temp.	Broken in two places.
71	Zr–U	Tensile test	Air	Room temp.	Broken inside gauge mark.
72	Zr–U	Tensile test	Argon	2600	Not broken but partially melted at one spot.

TABLE 5 (Continued)
E. Battelle Institute Samples

Sample No. G.T.C.	Composition	All samples subjected to rocket exhaust test in O_2, H_2, and H_2O atmosphere at 3500°R. and 0.25 atm. pressure unless otherwise noted	Comments
73	ZrH-10U (A.I. material)		Melted on face of cylinder.
74	1-ZrH-10U-2Ba		Sectioned and potted.
75	2-ZrH-10U-2Nb		Sectioned and potted.
76	3-ZrH-10U-5Sn		Sectioned and potted.
77	4-ZrH-10U-2Cu		Sectioned and potted.
78	5-ZrH-10U-2V		Sectioned and potted.
79	6-ZrH-10U-2Ca		Sectioned and potted.
80	7-ZrH-10U-2Nb-2Ba		Sectioned and potted.
81	8-ZrH-10U-2Sn-2Nb		Sectioned and potted.
82	9-ZrH-10U-5Cr		Sectioned and potted.
83	10-ZrH-10U		Sectioned and potted.
84	11-ZrH-10U-Ba		Sectioned and potted.
85	12-ZrH-10U-2W		Sectioned and potted.
86	13-ZrH-10U-2Ta		Sectioned and potted.
87	14-ZrH-10U-2Al		Sectioned and potted.
88	15-ZrH-10U-2Bi		Sectioned and potted.
89	16-ZrH-10U-5Sb		Sectioned and potted.
90	17-ZrH-10U (A.I. material)		Exposed to rocket 5 seconds, sectioned and potted.
91	18-ZrH_2-UO_2		Exposed to rocket 5 seconds, sectioned and potted.
92	19-ZrH_2-UC		Exposed to rocket 5 seconds, sectioned and potted.
93	20-ZrH_2-UN		Exposed to rocket 5 seconds, sectioned and potted.
94	21-ZrH-10U-2Sr		Exposed to rocket 5 seconds, sectioned and potted.
95	22-ZrH-10U-5Nb		Exposed to rocket 5 seconds, sectioned and potted.
96	23-ZrH-10U-5Th		Exposed to rocket 5 seconds, sectioned and potted.
97	24-ZrH-10U-2Ni		Exposed to rocket 5 seconds, sectioned and potted.
98	25-ZrH-10U-2Si		Exposed to rocket 5 seconds, sectioned and potted.
99	26-ZrH-10U-2Cr		Exposed to rocket 5 seconds, sectioned and potted.
100	27-ZrH-10U (A.I. material)		Exposed to rocket 2.5 seconds, sectioned and potted.
101	ZrH-10U-5Sn		Not tested.

TABLE 5 (Continued)

E. Battelle Institute Samples (Continued)

Sample No. G.T.C.	Composition	All samples subjected to rocket exhaust test in O_2, H_2, and H_2O atmosphere at 3500°R. and 0.25 atm. pressure unless otherwise noted	Comments
102	ZrH-10U-2Al		Exposed to rocket for 8 seconds, cylinder ablated on one end.
103	ZrH-10U-2W		Exposed to rocket for 8 seconds, cylinder ablated on one end halfway back.
104	ZrH-10U-2V		Exposed to rocket for 8 seconds, cylinder ablated on one end.
105	ZrH-10U-2Si		Not tested.
106	Unidentified alloy section		Specimen found down stream after test.
107	ZrH-UN		Section of isostatically compacted specimens found down stream.
108	ZrH-UC		Section of isostatically compacted specimens found down stream.
109	Probably ZrH-UO$_2$		Section of isostatically compacted specimens found down stream.
110	Probably ZrH-UO$_2$		Section of isostatically compacted specimens found down stream.
111	Suspected to be ZrH-UN		Section of isostatically compacted specimens found down stream.
112	Suspected to be ZrH-UN		Section of isostatically compacted specimens found down stream.

TABLE 5 (Continued)
F. Astropower, Inc. Samples
All Testing Performed in Arc Plasma Facility

Sample No.			Partial Pressures of Plasma Gases			
G.T.C.	Astropower	Composition	Argon(atm.)	Oxygen(atm.)	Nitrogen(atm.)	Comments
113	64	Zr-U	1.000	0	0	Mounted particles.
114	65	Zr-U	.667	0	.333	Mounted particles.
115	66	Zr-U	.667	.333	0	Mounted particles.
116(a)	29	Zr-U	.667	.333	0	Mounted particles.
116(b)	55	Zr-U	.705	0	0	Mounted particles.
117(a)	64	Zr-U	1.000	0	0	Mounted particles.
117(b)	65	Zr-U	.667	0	.333	Mounted particles.
117(c)	66	Zr-U	.667	.333	0	Mounted particles.
117(d)	H1	ZrH-U	4.400*	0	0	Mounted particles.
117(e)	H2	ZrH-U	4.384*	0.016*	0	Mounted particles.
117(f)	H3	ZrH-U	9.800*	4.900*	0	Mounted particles.

*Pressures measured in psia instead of atms.

APPENDIX II

ANALYSIS OF CHEMICAL REACTIONS OF A HYDRIDED
FUEL ELEMENT DURING RE-ENTRY

An analysis of the behavior of a zirconium-uranium alloy in a high temperature, air atmosphere environment shows that it oxidizes according to the parabolic rate law and absorbs both nitrogen and oxygen into it.[33,34,35] The oxide formed, which is ZrO_2, also absorbs oxygen and nitrogen, as is evidenced by the phase diagrams.[45] Initially, it is assumed that small alloy additions of uranium (say up to 4 atomic percent) do not change the fundamental behavior of zirconium in an oxidizing atmosphere. The data will be shown to be in essential agreement with this assumption.

A. FACTUAL INFORMATION

The data available for analysis consist of the following known items.

1. Weight gain measurements[10] continuous in time, on sample fuel element material specimens for:

   a. 100%, 50%, and 10% air atmosphere environment at one atmosphere of pressure. The dearth of air pressure in the 10% and 50% air cases was made up by the addition of argon gas. The argon is known not to react with the fuel element material.

   b. 500°C, 800°C, 1100°C, and 1400°C temperature environments were used with each of the atmospheres listed in a.

2. The starting compounds and reaction product for each of the weight gain experiments are known. These include:

a. Initial composition or weight percent of hydrogen, zirconium, and uranium.

b. The final composition, hydrogen, nitrogen, oxygen, zirconium, and uranium.

c. The coating formed on the sample specimen surfaces, i.e. ZrO_2.

3. The length of time required for the fuel elements to reach an essentially uniform temperature under the environmental conditions described in 1b above is known.

4. The rate of hydrogen evolution from the Zr-H-U material as a function of the temperature for the range given in 1b above, when heated in an argon atmosphere, is known.

5. The quantity of hydrogen that the fuel element material will maintain in an activated absorption state is essentially independent of the external hydrogen pressure,[41] varying roughly from the one-eighth to the one-fourteenth power of the external pressure at a given temperature.

6. The rate of oxidation is essentially independent of the external oxygen pressure, so long as oxygen is supplied at the outer surface of the oxide-nitride layer (which is formed on the material), as fast as it is used up at the interface between this layer and the fuel element proper.[37]

7. Phase diagrams for the activated absorption of oxygen in zirconium and zirconia are available.[46]

8. Insofar as the heat energy released due to the chemical reactions of oxygen and nitrogen with the fuel element material is concerned, the energy produced per unit weight gain of the fuel element material is essentially the

same for the two reactions, $Zr + O_2 \longrightarrow ZrO_2$ and $2Zr + N_2 \longrightarrow 2ZrN$. These are the principal reactions to be considered.[27] An X-ray analysis of the surface material produced on the fuel element material under simulated re-entry conditions[31] and during the weight gain experiments[10] shows that the surface material is ZrO_2.

9. Zirconium and dilute binary alloys of Zr with other metals will oxidize much more rapidly in an atmosphere containing a few percent water vapor than in a dry atmosphere.[34]

10. When the fuel element material is exposed to a heating environment similar to that that it would experience during re-entry, but containing an excess of water vapor,[47,48] the sample fuel elements being tested partially melted and ablated away during the tests.

11. Samples of fuel element materials, when subjected to varying arc-image heating rates and atmospheric pressures that simulate those that would be experienced by a fuel element along a variety of re-entry trajectories, do not lose their geometrical integrity.[31] However, they do lose hydrogen and do have coatings of ZrO_2 formed on their surfaces.

12. The solubilities of oxygen in Zr and ZrO_2 are approximately equal.[48]

13. When heated in an air atmosphere for long periods of time, the fuel element material exhibits "break-away" oxidation. Due to the large thicknesses of the oxide involved, this is not attributed to a mismatch in thermal expansion coefficients between the alloy and the oxide.

14. It can be shown analytically that the most rapid possible rate of oxidation (or other chemical reaction) in an ion diffusion controlled process is that rate described by the parabolic oxidation law.

78

B. MATHEMATICAL MODEL FOR CHEMICAL REACTIONS

1. Correction Factors for Weight Gain Measurements

The weight gain measurements made by ARF, described in Item 1 above, were made on short cylindrical samples (0.585 cm long, 1.905 cm diameter). Because the oxide layers formed on the surface of these test samples were thick, and because the oxidation rate laws are based on weight gains per unit area, it is necessary to correct the weight gain data for the fact that the surface area of the unreacted material decreases as the weight (thickness of the oxide layer) of the sample increases. By making use of the geometry of a cylinder, it can be shown that the area of the sample, $A(t)$, that remains at the time, t, and hence is available for oxidation is simply given by

$$A(t) = 2\pi (R - S) \left[(R - S) + 2(L - S) \right] \tag{91}$$

where R = initial cylinder radius,

L = one-half of the initial length of the cylinder, and

S = thickness of the metal that has been converted to a coating (i.e., an oxide and/or nitride).

It can also be shown in an analytical manner that if $f(t)$ is the fractional weight gain of the sample at the time, t, and K is the weight of the reacted compound containing one gram of the metal, then the value of S is the solution to the following relation:

$$S^3 - (L + 2R) S^2 + (R^2 + 2RL)S - \frac{R^2 L f(t)}{K - 1} = 0. \tag{92}$$

The total weight of the sample at time, t, is the initial weight, W_o, plus the weight $W_o f(t)$. The data on weight gain measurements were taken on a strip-chart which showed the integral weight gain as a function of time. Because the relative magnitudes of the possible reactions that took place during the data-gathering time interval, these data must be reduced to finite

difference form for the proper interpretation of the results. The weight gain per unit area during the ith time interval, Δt_i, can readily be shown to be given by

$$\Delta m_s (\Delta t_i) = \frac{\Delta f(\Delta t_i) W_o}{A(t')} \tag{93}$$

where $\Delta f(\Delta t_i)$ is the change in the fractional weight of the sample during the time interval, Δt_i, and $t' = t - \frac{1}{2}\Delta t_i$. It is clear that

$$\sum_{k=1}^{i} \Delta t_k = t, \tag{94a}$$

$$\sum_{k=1}^{i} \Delta m(\Delta t_k) = \Delta m_s(t), \text{ and} \tag{94b}$$

$$\sum_{k=1}^{i} \Delta f(\Delta t_k) = f(t). \tag{94c}$$

These equations are applicable to any cylinder that is undergoing a weight gain due to a surface reaction that forms a coating of products on the surface thereof. The quantity $f(t)$ is interpreted as the weight gain (or loss) due to the formation (or decomposition) of the surface coating.

2. Description of Reactions

The weight gain (or loss) of the element is due to oxidation and/or nitridation (Δm_s), to nitrogen and oxygen absorption (Δm_a), and to dehydriding (Δm_H), so that the total weight change at a given time is

$$\Delta m(t) = \Delta m_s + \Delta m_a - \Delta m_H. \tag{95}$$

The weight gain data, when corrected in accordance with eqs. (93) and (94), lead one to suspect that at first there is some loss of hydrogen and absorption of nitrogen and oxygen, together with oxidation. After some time has lapsed, the process follows a true parabolic law, and, finally, for the very thick coatings, exhibits breakaway oxidation. In view of the fact that

80

oxygen and nitrogen have almost identical atomic sizes and masses, no distinction will be made between them insofar as mass increases due to their absorption into the sample material during weight measurements are concerned. With this simplification, and in view of Item 8 above, eq. (95) can be written as

$$\Delta m(T, t, p) = \left[A_s t\right]^{1/2} e^{-Q/2T} + A_a p^{1/2} t e^{-E/T} - \Delta m_H(T, t). \tag{96}$$

Here, $R_g Q$ and $R_g E$ are activation energies, when R_g is the universal gas constant, A_s and A_a are constants, and p is the partial pressure of the component of the gas being absorbed. The first right-hand side term in this relation represents the parabolic chemical reaction law and the second the activated absorption law.[35]

a. Determination of activated absorption constants.-- The values of A_a and E are determined as follows. Holding T and t constant and letting p vary for two sets of t and T, eq. (96) shows that

$$\Delta m(T_1, t_1, p_1) - \Delta m(T_1, t_1, p_2) = A_a t_1 e^{-E/T_1} \left[p_1^{1/2} - p_2^{1/2}\right] \tag{97a}$$

and

$$\Delta m(T_2, t_2, p_1) - \Delta m(T_2, t_2, p_2) = A_a t_2 e^{-E/T_2} \left[p_1^{1/2} - p_2^{1/2}\right]. \tag{97b}$$

These two equations determine the values of A_a and E. The values of t to be used must be sufficiently small to assure that the absorption process is not seriously inhibited by the oxide coating that is being built up on the surface of the sample. Examination of the weight gain data show that Δm_a is only a few percent of Δm_s, being less than 1.7% weight gain in all cases. Its values are essentially masked by errors in the data and hence can be considered as negligible insofar as the present analysis is concerned. The oxygen and nitrogen absorption effects would be even less under actual re-entry conditions because of the low pressure in the boundary layer about the fuel element during the initial stages of oxidation.

b. <u>Determination of hydrogen loss rate</u>.--By heating the fuel element material in an argon atmosphere and noting the rate of hydrogen loss, it is immediately apparent that the loss rate is an exponentially decreasing one. This suggests the following differential equation:

$$\frac{d M_{Hr}}{dt} = (M_{Ho} - M_{Hr}) \lambda ,$$

where M_{Hr} is the amount of hydrogen that has been released per unit area from the sample speciment, M_{Ho} is the amount of hydrogen that was initially available for release (per unit area) at the temperature in question, and λ is a temperature dependent parameter. Integrating this expression and evaluating the constant of integration by making use of the boundary condition $M_{Hr} = 0$ at $t = 0$ gives

$$M_{Hr} = M_{Ho} (1 - e^{-\lambda t}) . \tag{98}$$

Making use of the dehydriding rates reported in reference 10, a plot of λ versus T can be obtained. This plot is a straight line whose equation is

$$\lambda = 1.01 \times 10^{-3} T - 1.92. \tag{99}$$

This relationship is valid for $T > 1900^{\circ}R$. Below this temperature, the loss rate can be considered to be zero for the practical problem at hand.

The hydrogen that is released diffuses through the oxide layer that is being formed on the surface of the fuel element material. The rate of loss through the oxide layer per unit area is governed by a diffusion equation of the form

$$\frac{d M_{H\ell}}{dt} = - a \text{ grad } C_H , \tag{100}$$

where $M_{H\ell}$ is the amount of hydrogen that has diffused through the oxide layer and escaped into

82

the surrounding environment, C_H is the hydrogen concentration, and a is the diffusion constant multiplied by the density of the oxide film. Since the concentration just outside the oxide surface is essentially zero, it follows that

$$\text{grad } C_H = \frac{M_{Hr} - M_{H\ell}}{\Delta m_s} .$$

(101)

Substituting eqs. (98) and (101) into (100) gives, upon rearrangement,

$$\frac{d M_{H\ell}}{dt} - \frac{a M_{H\ell}}{\sqrt{k_s t}} = - \frac{a M_{Ho}(1 - e^{-\lambda t})}{\sqrt{k_s t}}$$

(102)

where k_s is the parabolic rate constant, i.e.

$$k_s = A_s e^{-Q/T} .$$

(103)

This, then, is the differential equation describing the rate of hydrogen loss (per unit area) through the surface of the oxide coating.

To solve eq. (102), note that it is of the form

$$\frac{dy}{dx} + f(x)y = g(x)$$

(104a)

The complimentary solution (solution to homogeneous equation) is simply

$$y = C e^{-\int f(x)\, dx}, \quad C = \text{constant}.$$

(104b)

Letting $C = C(x)$, and using the method of variation of parameters, gives, upon differentiation and substituting into (104a),

$$C(x) = \int \left[g(x)\, e^{\int f(x)\, dx} \right] dx + \bar{A}$$

(104c)

where $\bar{A}$ is the constant of integration. Substituting eq.(104c) into (104b) gives

$$y(x) = \exp\left[-\int f(x)\, dx \right] \left\{ \bar{A} + \int g(x) \exp\left[\int f(x)\, dx \right] dx \right\} .$$

(104d)

Substituting eq. (102) into this general solution gives

$$\Delta m_H = M_{H\ell} = \exp\left[\int \frac{a\,dt}{\sqrt{k_s t}}\right] \left\{\bar{A} + \int \frac{a\,M_{Ho}(1-e^{-\lambda t})}{\sqrt{k_s t}} \exp\left[-\int \frac{a\,dt}{\sqrt{k_s t}}\right]dt\right\} \qquad (105)$$

Now, $\int (a/\sqrt{k_s t})\,dt$ is readily integrated to give $2a(t/k_s)^{\frac{1}{2}}$, thus, (105) becomes

$$\Delta m_H = \bar{A}\,e^{2a\sqrt{t/k_s}} - \frac{a\,M_{Ho}}{\sqrt{k_s}}\,e^{2a\sqrt{t/k_s}}\left[\int \frac{e^{-(\lambda t + 2a\sqrt{t/k_s})}}{\sqrt{t}}\,dt - \int \frac{e^{-2a\sqrt{t/k_s}}}{\sqrt{t}}\,dt\right] \qquad (106)$$

The last integral in eq. (106) is readily integrated, that is,

$$\int \frac{e^{-2a\sqrt{t/k_s}}}{\sqrt{t}}\,dt = \frac{\sqrt{k_s}}{a}\,e^{-2a\sqrt{t/k_s}} \qquad (107a)$$

If $q = t^{\frac{1}{2}}$ is substituted into the first integral in eq. (106), it becomes

$$\int \frac{e^{-(\lambda t + 2a\sqrt{t/k_s})}}{\sqrt{t}}\,dt = 2\int e^{-(\lambda q^2 + 2aq/\sqrt{k_s})}\,dq.$$

Then, let $u = \lambda q^2 + 2aq/\sqrt{k_s}$, to obtain

$$2\int e^{-u}\frac{du}{\sqrt{\left[\frac{a}{\lambda\sqrt{k_s}}\right]^2 + \frac{u}{\lambda}}} \,.$$

Integration by parts gives

$$2\,e^{-u}\sqrt{\left[\frac{a}{\lambda\sqrt{k_s}}\right]^2 + \frac{u}{\lambda}} - 2\int e^{-u}\sqrt{\left[\frac{a}{\lambda\sqrt{k_s}}\right]^2 + \frac{u}{\lambda}}\,du. \qquad (107b)$$

Now, change variables by letting $v^2 = \left[\frac{a}{\lambda\sqrt{k_s}}\right]^2 + \frac{u}{\lambda}$ in the integral of eq. (107b) to obtain

$$-2\int e^{-u}\sqrt{\left[\frac{a}{\lambda\sqrt{k_s}}\right]^2 + \frac{u}{\lambda}}\,du = -2\lambda e^{a^2/\lambda k_s}\int e^{-\lambda v^2}v(2v\,dv).$$

Integrating this expression by parts gives

84

$$2ve^{-(a^2/\lambda k_s + \lambda v^2)} - 2e^{-a^2/\lambda k_s} \sqrt{2\pi} \left[\frac{1}{\sqrt{2\pi}} \int e^{-(v\sqrt{\lambda})^2} dv \right] .$$

The bracketed expression is simply $\text{erf}(v\sqrt{\lambda})$. Substituting this into (107b) and changing variables back to t gives, upon simplification,

$$2(t^{1/2} + a/\lambda\sqrt{k_s}) e^{-(\lambda t + 2a\sqrt{t/k_s})} \left[1 + e^{-2a^2/\lambda k_s} \right] - 2\sqrt{2\pi} \ e^{-a^2/\lambda k_s} \text{erf}(\lambda t + a/\sqrt{\lambda k_s}) \quad (107c)$$

Substituting eqs. (107a) and (107c) into eq. (106) gives the complete primitive of eq. (102) as

$$\Delta m_H = \overline{A} \ e^{2a\sqrt{t/k_s}} + \frac{a \ M_{Ho} \ e^{2a\sqrt{t/k_s}}}{\sqrt{k_s}} \left\{ 2(t^{1/2} + a/\lambda\sqrt{k_s}) e^{-(\lambda t + 2a\sqrt{t/k_s})} \left[1 + \right. \right.$$

$$\left. e^{-2a^2/\lambda k_s} \right] - 2\sqrt{2\pi} \ e^{-a^2/\lambda k_s} \ \text{erf}(\sqrt{\lambda t} + a/\sqrt{\lambda k_s}) + \sqrt{\frac{k_s}{a}} \ e^{-2a\sqrt{t/k_s}} \right\} \quad (108)$$

The constant $\overline{A}$ can be evaluated by making use of the boundary condition that $\Delta m_H = 0$ at $t = 0$. This gives

$$\overline{A} = \frac{-a \ M_{Ho}}{\sqrt{k_s}} \left\{ (2a/\lambda\sqrt{k_s})(1 + e^{2a^2/\lambda k_s}) - 2\sqrt{2\pi} \ e^{-a^2/\lambda k_s} \ \text{erf}(a\sqrt{\lambda k_s} + \sqrt{k_s}/a) \right\} \quad (109)$$

Substitution of this value of $\overline{A}$ into eq. (108) gives the amount of hydrogen lost per unit area in a time t as

$$\Delta m_H(t) = \frac{a \ M_{Ho}}{\sqrt{k_s}} \ e^{2a\sqrt{t/k_s}} \left\{ \frac{-2a}{\lambda\sqrt{k_s}} (1 + e^{-2a^2/\lambda k_s}) + 2\sqrt{2\pi} \ e^{-a^2/\lambda k_s} \left[\text{erf}(\sqrt{\lambda t} \right. \right.$$

$$\left. + a/\sqrt{\lambda k_s}) - \text{erf}(a/\sqrt{\lambda k_s}) \right] + \frac{\sqrt{k_s}}{a} (1 - e^{-2a\sqrt{t/k_s}})$$

$$\left. + 2(\sqrt{t} + a/\lambda\sqrt{k_s}) (1 + e^{-2a^2/\lambda k_s}) \ e^{-(\lambda t + 2a\sqrt{t/k_s})} \right\} \quad (110)$$

The diffusion parameter must be determined experimentally. This is accomplished by measuring the quantity of hydrogen left in the sample specimens after they have been exposed to the weight gain tests. There was quite a spread in the initial weight percentages, M_{Ho}, of the test sample specimens, varying from approximately 1.4 weight percent to 1.7 weight percent. Because of this nonuniformity among the various specimens tested, the mean value of $M_{Ho} = 1.55$ weight percent was taken for determining a. Various sample specimens that had been exposed to the weight gain tests were analyzed for hydrogen content by vacuum fusion analyses. This results in a corresponding spread in the values of a. The value of a so determined is

$$a = A_H \, e^{-Q_H/T}, \text{ where } A_H = 0.10, \text{ and } Q_H = 1.84 \times 10^4. \tag{111}$$

Substituting these values and eq. (99) into eq. (102) gives the rate of hydrogen loss per unit area

$$\frac{d}{dt}\left[\Delta m_H(t)\right] = \frac{a \, \Delta m_H(t)}{t^{\frac{1}{2}} A_s \, e^{-Q_s/T}} - a \, M_{Ho}\left[1 - \exp(1.92 - 1.01 \times 10^{-3} T)\right]. \tag{112}$$

The value of $\Delta m_H(t)$ is given by eq. (112), and the value of M_{Ho} has to be known. For the particular samples used in the weight gain tests,

$$M_{Ho} = 1.55 \times 10^{-2} \frac{W_o}{A_{(o)}} = 1.69 \times 10^{-3} \text{grams/cm}^2.$$

The values of A_s and Q_s are to be taken from eq. (116) below.

c. Determination of the parabolic rate constant.--When the weight gain data, as modified by eq. (93), are plotted on log-log paper, the result is a family of parallel, straight lines for t greater than about 15 to 20 minutes, one line for each temperature (see Fig. 7). It is readily determined that the process involved is parabolic in nature, that is, each of the lines can easily be fitted by an equation of the form

$$\Delta m_s^2 (T, t) = k(T)t + C(t). \tag{113}$$

By holding T constant and varying t, one can calculate the value of $k(T)$, i.e.

$$\Delta m_s^2 (T, t_1) - \Delta m_s^2 (T, t_2) = k(T) (t_1 - t_2). \tag{114}$$

Here, it has been assumed that $C(t)$, which arises from Δm_a and Δm_H is actually constant for

large values of t, say $t > 20$ minutes. The fact that the family of lines are truly parabolic

supports this position. That is, if there are changes in Δm_a and Δm_H for large values of t, they

are overshadowed by Δm_s to within the limits of the accuracy of the data.

The reaction rate constant is known to obey Arrhenius' equation,[28] that is,

$$k(T) = A e^{-Q/T}. \tag{115}$$

The value of k is determined from eq. (114), using the temperatures $1390^\circ R$, $1930^\circ R$, $2470^\circ R$,

and $3010^\circ R$. There is a phase change in the fuel element material at approximately $2040^\circ R$.

This phase change changes the value of k. If log k is plotted versus $1/T$ for the $1390^\circ R$ and

$1930^\circ R$ points and for the $2470^\circ R$ and $1930^\circ R$ points, the pair of straight lines connecting these

two pairs of points cross at the phase change temperature (see Fig. 8). This is the result ex-

pected, and it lends even greater confidence to the values of A and Q so determined. They are

$$A_s = 0.356 \ (gms^2/cm^4\text{-}min), \ \ Q_s = 2.59 \times 10^4, \ \ for \ T \leq 2040^\circ R, \tag{116a}$$

$$A_s = 92.5 \ (gms^{-1}/cm^4\text{-}min), \ \ Q_s = 3.79 \times 10^4, \ \ for \ T \geq 2040^\circ R. \tag{116b}$$

With these parameters determined, the mass increase at any time can now be determined by

eq. (95) for any combination of the sets of variables (T, t). Also, the rate of hydrogen evolution

is determined by using the results of eq. (116) in eq. (112).

REFERENCES

1. J. L. Raymond and T. B. Gaber, "On the Stability of a Circular Cylinder at Hypersonic Speeds," RAND Paper D-723 (Jun. 9, 1956).

2. W. T. Davey and C. E. Gribsby, "Stability Characteristics of Cones and Cylinders at Large Angles of Attack at Mach Number 2.87," Aeronutronics Report No. U-540(Aug.59).

3. "Investigation of Re-Entry Destruction of Nuclear Auxiliary Power Plant," AFSWC-TR-61-69.

4. R. J. Vidal and C. E. Wittliff, Third Int. Rarefied Gas Dynamics Symposium, Vol. 2, Academic Press, N. Y., (1963), pp. 343-378.

5. J. A. Fay and F. R. Riddell, J. Aero, Sci., Vol. 25, pp. 73-85 (Feb. 1958).

6. P. H. Rose and Affenhartz, AVCO Res. Rept. No. 114 (Aug. 1959).

7. S. Georgiev, "Hypersonic Ablation and Interpretation of Test Results," AVCO Res. Rept. No. 99 (Oct. 1960).

8. H. S. Carslaw and J. C. Jaeger, Conduction of Heat in Solids, P. 203, Oxford at the Clarendon Press (1959).

9. J. L. Raymond, "The Rotational Motion of a Rod Entering the Earth's Atmosphere," RAND RM-2629 (Oct. 1, 1960).

10. J. C. Hedge, J. I. Lang, E. Howe, and R. Elliott, "High Temperature Property Study for Re-entering NAP Systems," AFSWC-TDR 63-17 (June 1963).

11. J. A. Penland, "Aerodynamic Characteristics of a Circular Cylinder at Mach Number 6.86 and Angles of Attack up to $90°$," NACA Tech. Note 3861, (June 1957).

12. N. Am. Aviation, Inc., Report, "Flight Test Criteria for Re-entering NAP Systems," AFSWC-TDR-62-83.

13. H. K. Cheng, CAL Rept. No. AF-1285-A-7 (1961).

14. C. B. Cohen and E. Reshotko, "Similar Solutions for the Compressible Laminar Boundary Layers with Heat Transfer and Pressure Gradient," NACA TN 3325 (1955).

15. O. K. Tewfik and W. H. Giedt, J. A. S., Vol. 27, pp. 721-729 (1960).

16. I. Beckwith, NACA RM 55F09 (1955).

17. H. K. Cheng and A. Chang, CAL Rept. No. AF-1515-A-1 (1962).

18. E. R. G. Eckert, *J. Aeronaut. Sci.*, Vol. 22, pp. 585-587 (Aug. 1955).

19. W. D. Hayes and K. F. Probstein, *Hypersonic Flow Theory*, Academic Press, N. Y., p. 296 (1959).

20. N. B. Cohen, "Correlation Formulas and Tables of Density and Some Transport Properties of Equilibrium Dissociating Air For Use in Solutions of the Boundary-Layer Equations," NASA TN D-194 (1960).

21. "Equations, Tables, and Charts for Compressible Flow," Ames Staff, NACA Rept. 1135 (1953).

22. G. G. Chernyi, *Introduction to Hypersonic Flow*, p. 214, Acad. Press, N. Y. (1961).

23. N. H. Kemp, P. H. Rose, and R. W. Detra, "Laminar Heat Transfer Around Blunt Bodies in Dissociated Air," AVCO Research Report No. 15 (1958).

24. R. W. Detra and H. Hidalgo, "Generalized Heat Transfer Formulae and Graphs," AVCO Research Report No. 72 (1958).

25. K. F. Probstein, "Invicid Flow in the Stagnation Region of Very Blunt Nosed Bodies at Hypersonic Flight Speeds," WADC TN 56-395 (Sept. 1956).

26. C. E. Wittliff and J. T. Curtis, "Normal Shockwave Parameters in Equilibrium Air," CAL Rept. No. CAL-111 (Nov. 1961).

27. O. Kubaschewski and B. E. Hopkins, *Oxidation of Metals and Alloys*, Academic Press, Inc., London (1953).

28. J. S. Dunn, *Proc. Roy. Soc. A111*, p. 203 (1926).

29. E. A. Gulbransen and K. F. Andrew, "Oxidation of Zirconium Between 400 and 800° C.," *J. of Metals*, pp. 394-400 (Apr. 1957).

30. C. E. Wicks and F. E. Block, "Thermodynamic Properties of 65 Elements, Their Oxides, Halides, Carbides, and Nitrides," Bulletin 605, BuMines (1963).

31. Fred E. Littman, "Zirconium-Uranium Combustion Study," SWC TDR 63-15 (Dec. 1962).

32. R. D. Elliott, "Aerospoce Safety Re-entry Analytical and Experimental Program SNAP 2 and 10A," (Interim Report), NAA-SR-8303 (Sept. 1963).

33. North American Aviation Final Report, SWC TDR 63-14 (April 1963). (See p. 73 and pp. 202,203.)

34. E. T. Hayes and A. H. Roberson, "Some Effects of Heating Zirconium in Air, Oxygen, and Nitrogen," *Trans. of the Electrochemical Society*, Vol. 96, p. 1212 (1949).

35. E. A. Gulbransen and K. F. Andrew, J. Metals Transactions, Vol. 185, p. 515 (1949).

36. E. A. Gulbransen and K. F. Andrew, Trans AIME Journal of Metals, Vol. 9, p. 394 (1957).

37. R. G. Charles, S. Barnartt, and E. A. Gulbransen, Trans. Am. Inst. Mining Met. Engrs., Vol. 212, 101 (1958).

38. J. Belle and M. W. Mallett, Jour. of the Electrochemical Soc., Vol. 101, p. 339 (1954).

39. P. Kofstad, Acta. Chem. Scand., Vol. 12, 701 (1958).

40. A. Draunieks, Am. Chem. Soc. Jour., Vol. 72, 3568 (1950).

41. D. F. Atkins, "Dissociation Pressures of Hydrided Zirconium-Uranium Alloys," NAA-SR-4245, c. 16A.

42. Irving Weinstein, "Heat Transfer and Pressure Distributions on a Hemisphere-Cylinder and a Bluff-Afterbody Model in Methane-Air Combustion Products and in Air" (See Figs. 11 and 12), NASA TN D-1503 (December 1962).

43. Donald M. Kuehn, "Experimental and Theoretical Pressures on Blunt Cylinders for Equi-librium and Non-equilibrium Air at Hypersonic Speeds," NASA TN D-1979 (Nov. 1963).

44. Fred E. Littman, Paper presented at the AFWL Contractor's Meeting at Kirtland AFB, N. M., on Jan. 21, 1964.

45. E. J. Opik, Physics of Meteor Flight in the Atmosphere, Interscience Publishers, Inc., N. Y. (1958).

46. R. F. Domagala and D. J. McPherson, "Phase Diagrams of Zirconium-Base Binary Al-loys, The Zirconium-Oxygen System," USAEC Contr. No. AT(11-1)-149, Rept. No. 10, ARF of Ill. Inst. of Tech., 1953.

47. Ellis L. Foster, Jr., "Burn-Up Enhancement for Re-entering NAP Systems," RTD-TDR-63-3054 (Oct. 1963).

48. W. J. Fleming, Jr. and R. A. Rindal, "The Response of Nuclear Auxiliary Power Unit Fuel Rods to Simulated Re-entry Heating," AFSWC-TDR-63-52 (May 1963).

DISTRIBUTION

No. cys.

HEADQUARTERS USAF

1   Hq USAF (AFCOA), Wash, DC 20330

1   USAF Dep, The Inspector General (AFIDI), Norton AFB, Calif 92409

1   USAF Directorate of Nuclear Safety (AFINS), Kirtland AFB, NM 87117

MAJOR AIR COMMANDS

1   AFSC (SCCP), Andrews AFB, Wash, DC 20331

1   AUL, Maxwell AFB, Ala 36112

AFSC ORGANIZATIONS

1   Systems Engineering Group, Research & Technology Division, AFSC, ATTN: SEPRR, Wright-Patterson AFB, Ohio 45433

1   RTD (RTN-W, Lt Col Munyon), Bolling AFB, Wash, DC 20332

SSD, AF Unit Post Office, Los Angeles 45, Calif 90045

1   (SSTRE)

1   (SSZMS)

KIRTLAND AFB ORGANIZATIONS

1   AFSWC (SWEH), Kirtland AFB, NM 87117

AFWL, Kirtland AFB, NM 87117

10   (WLIL)

1   (WLRP)

1   (WLAS)(ATTN: Lt R. W. Obermeyer)

3   (WLDN)

OTHER AIR FORCE AGENCIES

3   Director, USAF Project RAND, via: Air Force Liaison Office, The RAND Corporation, ATTN: Miss Mary Romig, 1700 Main Street, Santa Monica, Calif 90406

NAVY ACTIVITIES

1   US Naval Weapons Evaluation Facility (NWEF) (Code 404), Kirtland AFB, NM 87117

OTHER DOD ACTIVITIES

Director of Defense Research & Engineering, The Pentagon, Wash, DC 20330

2   (Lt Col Roy C. Weidler)

2   (James E. Blower)

DISTRIBUTION (cont'd)

No cys.

20 Hq Defense Documentation Center for Scientific and Technical Information (DDC), Bldg 5, Cameron Sta, Alexandria, Va 22314

AEC ACTIVITIES

US Atomic Energy Commission, Mail Station G-017, Wash, DC 20545

4 (DRD/Asst Director for Compact Reactor Systems)

4 (DRD/Asst Director for Nuclear Safety)

6 Sandia Corporation (Information Distribution Division), Sandia Base, NM 87115

1 US Atomic Energy Commission, Canoga Park Area Office, ATTN: Manager, CPAO/Mr. J. Levy, Canoga Park, Calif

OTHER

1 OTS, Department of Commerce, Wash 25, DC

3 General Technologies Corp., ATTN: Mr. J. D. Graves, 2302 Willowood Lane, Alexandria, Va

1 Official Record Copy (Lt Pourciau, WLDN)